

1-1-2013

Enhancing Radiotherapy Using Ultrasound And Microbubbles With Gold Nanoparticles

Amanda T.L. Tran
Ryerson University

Follow this and additional works at: <http://digitalcommons.ryerson.ca/dissertations>



Part of the [Biological and Chemical Physics Commons](#)

Recommended Citation

Tran, Amanda T.L., "Enhancing Radiotherapy Using Ultrasound And Microbubbles With Gold Nanoparticles" (2013). *Theses and dissertations*. Paper 1705.

ENHANCING RADIOTHERAPY USING ULTRASOUND AND MICROBUBBLES WITH
GOLD NANOPARTICLES

by

Amanda Thu Lee Tran
B.Sc. Ryerson University, 2010
Toronto, Canada

A thesis

presented to Ryerson University

in partial fulfillment of the
requirements for the degree of
Master of Science
in the Program of
Biomedical Physics

Toronto, Ontario, Canada, 2013

© Amanda Thu Lee Tran, 2013

Author's Declaration

I hereby declare that I am the sole author of this thesis. This is a true copy of the thesis, including any required final revisions as accepted by my examiners.

I authorize Ryerson University to lend this thesis to other institutions or individuals for the purpose of scholarly research.

I further authorize Ryerson University to reproduce this thesis by photocopying or by other means, in total or in part, at the request of other institutions or individuals for the purpose of scholarly research.

I understand that my thesis may be made electronically available to the public.

Amanda Thu Lee Tran

Abstract

Enhancing radiotherapy using ultrasound and microbubbles with gold nanoparticles

Amanda Thu Lee Tran
Master of Science, Biomedical Physics
Ryerson University, 2013.

Gold nanoparticles (AuNPs) have been shown to enhance the local radiation dose in tumour mice models. Although AuNPs can be delivered to tumours through enhanced permeability and retention (EPR) effect, delivering of AuNP for therapeutic effect has been proven to be challenging. The application of ultrasound and microbubbles (USMB) has been shown to increase the delivery of genetic material, macromolecules, and chemotherapeutic agents. The hypothesis driving this research is that ultrasound and microbubbles can increase uptake of AuNPs in cells. The results suggest that AuNPs, and USMB aid in its delivery to increase cell death upon irradiation. An improvement of ~ 22 fold was observed with the combined treatment compared to radiation only, implying synergism. In addition, USMB and radiation exhibited an increase in cell death. Cell viability was ~3-4% and is dependent on AuNP concentration, shape and location. Further investigation of this concept was done *in vivo*.

Acknowledgments

I would like to thank the most patient person I have ever had the pleasure in working with, my supervisor and mentor, Dr. Raffi Karshafian. Without his guidance and positive attitude, this milestone in my life would have not been possible. I began this journey with very little knowledge of the research field and through my time in Dr. Karshafian and Dr. Czarnota's lab, I can honestly say that I have gain a true passion for science. Thank you for taking me under your wing; your guidance has made me an even more confident and curious scientist.

Many thanks to my supervisory committee, Dr. Michael Kolios, Dr. Greg Czarnota, and Dr Jean-Philippe Pignol, who have helped guide me through my experience and prepare me for the completion of this degree. I would like to extend my gratitude to Dr. Gregory Czarnota, for providing the facilities in making this project possible.

I must also thank my fellow lab mates, Firas Almarsi, Christine Tarapacki, Robert Earl, Edna Sacay, Priscilla Lai, and Anoja Giles who have provided support during early mornings and long nights of failed and successful experiments. I remember the countless times I stared at an equation for hours and eventually just handed it over to you.

To my loving family and friends for supporting me through my academic journey and putting up with my many complaints.

My Gabriel Wolfaardt, for standing by me through it all.

Dedication

To my mother, my personal cheerleader.

TABLE OF CONTENTS

Abstract	iii
Acknowledgments	iv
Dedication	v
TABLE OF CONTENTS	vi
Symbols & Abbreviations	viii
LIST OF TABLES	ix
LIST OF FIGURES.....	x
Chapter 1	1
INTRODUCTION	1
1.1 – Radiotherapy.....	2
1.2 – Radiosensitizers and gold nanoparticles (AuNP)	3
1.2.1 – Physics of metal-enhanced radiotherapy	4
1.2.2 – AuNP size and concentration dependence	5
1.2.3 – AuNP local dose delivery enhancement dependent on energy	5
1.2.4 – AuNP delivery.....	7
1.2.5– Increasing AuNP delivery	8
1.3 – The physics of ultrasound.....	9
1.3.1 – Ultrasound in imaging and therapy	9
1.3.2 – Ultrasound and microbubbles	10
1.3.3 – Sonoporation	12
1.3.4 – Mechanism of sonoporation	13
1.3.5 – Radiosensitization of ultrasound-microbubble and possible mechanism	15
1.4 – Hypothesis	15
1.5 - References	17
Chapter 2	23
<i>IN VITRO</i> STUDY	23
Abstract	23
2.1 – Introduction	25
2.2 – Materials and Methods: in vitro cell suspension.....	27
2.2.1 - <i>In vitro</i> cell model.....	27
2.2.2 – Gold nanoparticles (AuNP)	28

2.2.3 - Ultrasound and microbubble treatment	28
2.2.4 – Radiotherapy (XRT)	29
2.2.5 – Clonogenic assay	30
2.2.6 – Analysis	30
2.3 – Results	31
2.3.1 – AuNP Spheres with USMB and XRT	31
2.3.2 – AuNP Rods with USMB and XRT	32
2.3.3 – Synergism of combined treatments	34
2.4 – Discussion	36
2.4.1 – Gold nanoparticle concentration and location significance	37
2.4.2 – Mechanism(s) associated with radioenhancement	38
2.4.3 – AuNP toxicity	40
2.4.4 – Limitations	40
2.5 – Conclusions	41
2.6 – References	42
2.7 – Appendix	48
Chapter 3	50
SUMMARY & FUTURE WORK	50
3.1 – Summary	50
3.2 – Future work	51
3.1 – Material and Methods: <i>in vivo</i> animal model	52
3.1.1 – <i>In vivo</i> animal model	52
3.1.2 – Gold nanoparticles (AuNP)	53
3.1.3 – Ultrasound and microbubble treatment	53
3.1.4 – Radiotherapy (XRT)	53
3.1.5 – Growth Delay	53
3.1.6 – Histology	54
3.1.7 – Ultrasound Imaging	54
3.2 – Results & Discussion	55
3.2.1 – Histology images	55
3.2.2 – Growth Delay	58
3.2.3 – References	59

Symbols & Abbreviations

[Au] - gold concentration

AuNP - gold nanoparticles

DEF - dose enhancement factors

DNA – deoxyribonucleic acid

EPR effect - enhanced penetration and retention effect

H&E - hematoxylin and eosin

IUdR – Iododeoxyuridine

MC – Monte Carlo

MI – mechanical index

MV - megavolt

nps - nanoparticles

PEG - polyethylene glycol

SCID - severe combined immunodeficient

UCA – ultrasound contrast agents

USMB - ultrasound and microbubbles

V_A – calculated additive viability

V_C - combined experimental viability

XRT - irradiation

LIST OF TABLES

Table 2.1: A summary of the Bliss independence criterion T-test comparison (shown in Figure 2.4 and Figure 2.5) on spherical AuNPs where ✓ represents synergistic effects, and + represents additive effects.	48
Table 2.2: A summary of the Bliss independence criterion T-test comparison (shown in Figure 2.4 and 2.5) on rod shaped AuNPs where ✓ represents synergistic effects, and + represents additive effects.	48

LIST OF FIGURES

Figure 1.1: Schematic of a high Z material atom undergoing the photoelectric effect (left) where an electron is ejected out, causing electrons to fall from higher orbits producing an Auger cascade (right) (Reprinted from Goorley & Nikjoo, 2000).	4
Figure 1.2: Enhanced permeability and retention effect. Nanoparticles are able to enter into the tumour region via leaky tumour vasculature, allowing local uptake (adapted from Peer et al., 2007).	7
Figure 1.3: An illustration of a microbubble in an ultrasound field at a) low and b) high pressures. At low pressures, stable oscillation occurs (shaded circles) when its resonant, where at higher pressures, transient cavitation occurs when the inertial energy of the fluid surrounding the microbubble during compression causes the gas to diffuse out, forcibly collapsing the bubble (adapted from Newman & Bettinger, 2007).	11
Figure 1.4: Schematic diagram of ultrasound and microbubble induced sonoporation where a) when microbubbles are placed in an ultrasound field, the microbubbles undergo oscillation causing the phenomenon know as sonoporation. This b) allows macromolecules to c) enter the intracellular matrix, eventually d) resealing.	13
Figure 2.1: A schematic diagram of the ultrasound exposure apparatus. Cells are placed within the chamber and exposed to set acoustic conditions (Reprinted from Karshafian et al., 2009).....	29
Figure 2.2: Clonogenic viability of MDA-MB231 cells exposed to 12nm AuNP spheres were normalized to the control. a) Two different concentrations of AuNP, USMB fixed at 0.5MHz frequency pulses with 570kPa negative peak pressure and 3.3% (v/v) microbubbles, and a 160kVp 2Gy single radiation dose and their combinations are shown. The asterisks signify its statistical significance in comparison to samples without AuNPs, 0 nps/mL concentration. These samples were centrifuged, removing gold within the solution before irradiation. Cell viability of AuNP, USMB, and XRT combined treatments with gold in solution is represented in b). The asterisks in Figure 2.2b) represents its statistical significance (P< 0.05) compared with its corresponding condition in Figure 2.2a).	32
Figure 2.3: Clonogenic viability of MDA-MB231 cells exposed to 12 by 44nm rods shaped AuNPs normalized with control. Two different concentrations of AuNP, USMB fixed at 0.5MHz frequency pulses with 570kPa negative peak pressure and 3.3% (v/v) microbubbles, and a 160kVp 2Gy single radiation dose and their combinations are shown. The asterisks signify its statistical significance in comparison to samples without AuNPs, 0 nps/mL concentration. These samples were centrifuged,	

removing gold in the solution before irradiation. b) Represents the cell viability of rod shaped AuNPs, USMB, and XRT with gold in solution. The asterisks signify the statistically significant ($P < 0.05$) different to its corresponding treatment without gold in solution in Figure 2.3a)..... 33

Figure 2.4: The calculated additive effect (V_A) of AuNP, USMB, and XRT on a) spherical AuNPs and b) rod shaped AuNPs. The asterisks identify the treatments that have a statistically significant $V_C > V_A$ with $P < 0.05$ 35

Figure 2.5: The calculated additive effect (V_A) of different permutations of AuNP+USMB+XRT for a) spherical AuNPs and b) rod shaped AuNPs. The asterisks identify the treatments that have a statistically significant $V_C > V_A$ with $P < 0.05$ 36

Figure 2.1i – Schematic of possible biomechanisms occurring during the combined treatment of AuNP+USMB+XRT. a) The nanoparticle, microbubble, and cell suspension is exposed to ultrasound, causing b) sonoporation to occur, aiding in uptake. This increase in uptake c) improves local dose delivery and USMB radiosensitization, upon radiation to increase cell death. 49

Figure 3.1: Representative hematoxylin and eosin stains for the untreated control, AuNPs, USMB, XRT, AuNP+USMB, AuNP+XRT, USMB+XRT, and AuNP+USMB+XRT. Images were taken at 1x magnification with a light microscope. 56

Figure 3. 2: H&E stains of MDA-MB 231 mice tumours with different AuNP concentrations used with the combined treatment of AuNP+USMB+XRT. From top to bottom: 1.4mg/kg, 2.8mg/kg, and 3.8mg/kg of 50nm spherical PEG-AuNP used with the combined treatment with ultrasound and microbubbles and radiation (n=4). Images were taken at 1x magnification with a light microscope. 57

Figure 3.3: Growth delay curve of tumour growth post treatments normalized with untreated control (n=4). All microbubble treatments were done with 3% (v/v), with an AuNP dose of 2.8mg/kg and 2Gy X-ray radiation. 58

Chapter 1

INTRODUCTION

The therapeutic effect of radiotherapy has been shown to improve with the addition of gold nanoparticles (AuNPs) by ~ 3 fold or less (Kong *et al.*, 2008; Zhang *et al.*, 2008). AuNPs have been investigated for its high atomic (Z) number and relatively inert nature. These characteristics have made them a potential radioenhancer capable of locally delivering radiation within its proximity (Hainfeld *et al.*, 2006; Popovtzer *et al.*, 2008).

Delivery of AuNPs to cancerous tissues can be achieved through endocytosis *in vitro* (Chithrani *et al.*, 2006; Trono *et al.*, 2011) and through the enhanced permeability and retention effect (EPR effect) *in vivo*, to be preferentially taken up into tumours in mice. This has led to improvements in tumour growth control following radiotherapy (Hainfeld *et al.*, 2008; Kennedy *et al.*, 2011). However, challenges arise when delivering AuNPs to the target with optimal efficiency. AuNPs that are delivered via intravenous injections suggest that biodistribution of AuNP greatly resides within the bloodstream compared to the tumour and tumour peripheries post 5 minutes injection, (Hainfeld *et al.*, 2004). Although AuNP uptake is dependent on size, shape, and AuNP concentration, poor AuNPs delivery can be partially addressed through coating, biological targeting, and most recently, ultrasound and

microbubble mediated sonoporation (Chattopadhyay *et al.*, 2010; Hauck *et al.*, 2008; Tarapacki *et al.*, 2012.)

Ultrasound and microbubbles (USMB) have been shown to improve therapeutic efficacy of biologically active molecules through intracellular delivery (Iwanaga *et al.*, 2007). This thesis will investigate the use of microbubbles and ultrasound and its ability to increase cell permeability, a phenomenon known as *sonoporation*, and aid in enhancing radiation dose with AuNPs. Consequently, determining concentration and size factors with the combined treatment of AuNP + USMB + XRT in an *in vitro* (Chapter 2) and *in vivo* setting (Chapter 3) will be investigated.

1.1 – Radiotherapy

Radiotherapy remains a major therapeutic modality in cancer treatment with approximately 50% of all cancer patients receive radiation therapy. The primary goal of radiotherapy is the delivery of a lethal dose of radiation to a tumour with the concomitant sparing of surrounding healthy tissues. Much of the recent effort to attain this goal has been concentrated in two distinct categories, namely, conforming the delivered dose to the tumour volume, and enhancing the sensitivity of the tumour to therapeutic radiation.

The ability to conform radiation dose to the tumour has considerably improved with the use of intensity-modulated radiotherapy, proton radiotherapy, and modulated arc radiotherapy (Polf *et al.*, 2011; Webb, 2003; Yu & Tang, 2011). Radiation therapies with photon, electron, proton or neutron interactions have been employed extensively for treatment of nearly all types of solid tumours. A limiting factor of this method is the lack of contrast in the absorption of ionizing radiation between healthy and cancerous tissue (Webb, 2003). While different means of beam delivery methods are continuously being refined, other methods are being considered.

1.2 – Radiosensitizers and gold nanoparticles (AuNP)

Radiosensitizers may be used to locally enhance the delivery of the radiation dose at a cellular level, depending on the agent. Radiosensitizers are divided into two categories, apparent and true radiosensitizers. Apparent radiosensitizers are toxic agents that are effective in situations where radiation alone is less potent. True radiosensitizers such as analogues of purines (mercaptopurine) and pyrimidines (bromodeoxyuridine and iododeoxyuridine (IUdR)) promote direct and indirect DNA damage effects of radiation. Gold nanoparticles is an example of one that acts as both a conventional and non-conventional radiosensitizer where its high atomic number (Z) value improves local radiation dose.

The increase of dose when high-Z materials were within proximity of the targeted area was first realized 30 years ago. Chromosomal damage was noticed in circulating lymphocytes from patients that were undergoing iodine contrast angiography (Matsudaira *et al.*, 1980). Direct injection of iodine prior to radiation suppressed the growth of tumours in mice by 80% at low energies (Mello *et al.*, 1983). To utilize the radiosensitivity caused by iodine contrast agents, IUdR was introduced into cellular DNA, *in vitro* (Nath *et al.*, 1990). IUdR was able to achieve an increase of cell death of ~3 fold post radiation. However, dividing DNA is required to replace 20% or greater of cellular thymine with IUdR in an *in vivo* setting poses a challenge. This was demonstrated in preclinical phase I trials showing a decrease in its radiotherapeutic advantage (Kinsella *et al.*, 2000).

Since gold absorbs ~3 times more than iodine at 20 and 100 keV (Hainfeld *et al.*, 2008) gold may be more favourable for its potential as a radiosensitizer compared to iodine. Several recent studies have focused on the use of AuNPs to increase the sensitivity of tumours irradiated with clinical x-ray beams (Chithrani, *et al.*, 2010; Mesbahi, 2010). Both theoretical and *in vitro* and *in vivo* studies with AuNP treated tumours coupled with x-ray therapy have shown an increase in cell death (Hainfeld *et al.*, 2004) .

1.2.1 – Physics of metal-enhanced radiotherapy

When a material is exposed to x-rays, a number of processes may occur. With AuNPs, due to its high Z value ($Z=79$), the processes that are of importance include: the production of x-rays, the photoelectric effect, Auger cascade, and Compton scattering.

The photoelectric effect varies as Z^3/E^3 , where E is the incident photon energy required to eject an electron, and Z is the atomic number. Upon irradiation, high Z materials that result in increased photoelectric absorption cross-section, produces atoms in excited states and provides a conformal energy deposition surrounding the material. This causes rearrangement of electrons falling from higher orbits, generating the emission of a localized spray of radiation at a microscopic scale known as an Auger cascade (Pignol *et al.*, 2003). The localized dose of radiation is also caused by photoelectrons and characteristic X-rays (Carter *et al.*, 2007). Since the low energy electrons are short-range and are produced in large amounts by ionizing radiation, AuNPs have the potential localize radiation energy to the DNA of cancer cells. The effectiveness of this radiosensitization process varies widely with nanoparticle size, concentration and localization, as well as with source energy.

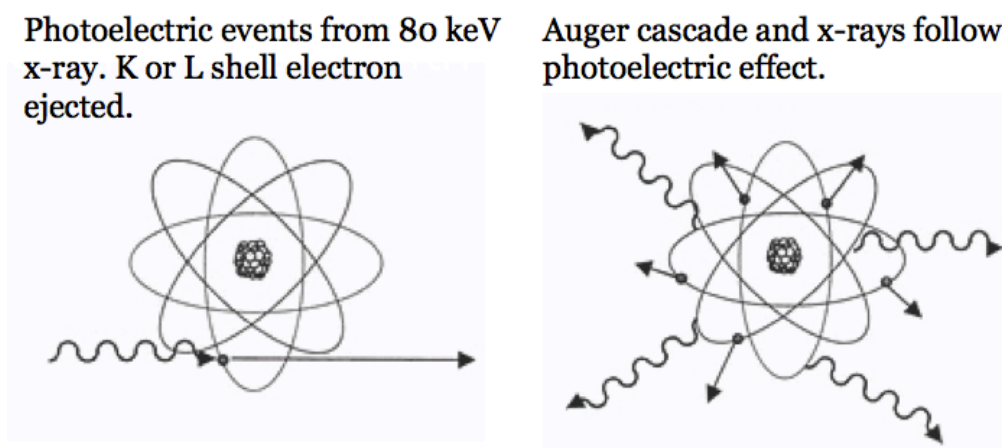


Figure 1.1: Schematic of a high Z material atom undergoing the photoelectric effect (left) where an electron is ejected out, causing electrons to fall from higher orbits producing an Auger cascade (right) (Reprinted from Goorley & Nikjoo, 2000).

1.2.2 – AuNP size and concentration dependence

The hydrophobic nature of the semi-permeable lipid bilayer of a cell membrane prevents solutes and large ions to diffuse across. However, depending on the type and size of the molecule, such particles can be taken up by a process known as endocytosis. The engulfing of the particle is done by means of pinching of the plasma membrane to form a pit for internalization. The ability to be made in a range of sizes best for tumour penetration and delivery gives AuNPs a major advantage. However, not all sizes are practical; particles of 1-2nm exhibited toxic side effects *in vitro*, where AuNPs of greater size were comparatively non toxic (Pan *et al.*, 2007).

Studies have shown that AuNP accumulation *in vitro* is primarily due to endocytosis and its non-specific absorption of proteins, and is important for maximal intracellular uptake (Chithrani *et al.*, 2006; Pan *et al.*, 2007; Trono *et al.*, 2011). The ideal AuNP size and shape is dependent on its use. It is also able to form a variety of shapes for specific purposes such as phototherapy. Rod shaped AuNPs tuned to absorb 810nm wavelengths laser light can result in local tissue coagulation, ablating tumour tissue (Dreaden *et al.*, 2011; Huang & El-Sayed, 2010). However, with phototherapy, penetration depth remains a challenge and rod shaped AuNPs are not ideal in optimal passive accumulation intracellularly. The shape and size which provides maximum nanoparticle per cell was determined to be spherical 50nm AuNPs, ultimately reaching a plateau with increased concentrations at 20 μM (Chithrani *et al.*, 2006). However this may be dependent on cell line, since a plateau was not observed at concentrations of 94 μM (Trono *et al.*, 2011).

1.2.3 – AuNP local dose delivery enhancement dependent on energy

Although the concentration and characteristics of AuNPs have varied in published studies, kilovolt radiosensitization has usually been attributed to increased photon absorption in high-Z materials, such as gold, in contrasted to soft tissue. In the kilovoltage region, gold has an attenuation coefficient two

orders of magnitude or greater than that of soft tissue providing a potential to significantly increase the dose deposited within a tumour (McMahon et al., 2008). *In vitro* models and *in vivo* tumour growth delay paired with AuNPs have been shown to decrease tumour growth and increase tumour cell death ((Hainfeld et al., 2010; Jain et al., 2011). However, this improvement is greatly dependent on the energy used and is limited to the kilovoltage region. Although some cancer patients are treated at kV energies with brachytherapy (ie: Iodine-125 at 35.5 keV), unsealed radioisotopes (ie: Iodine-131, at 364 keV), or intraoperative radiotherapy treatments during surgery, megavoltage (MV) X-rays are essential for skin sparing and adequate dose deposition to the region of interest (McMahon et al., 2008).

In the MV region, used by traditional linear accelerators, no difference in absorption coefficients between soft tissue and heavy elements can be observed (Cho, 2005). Monte Carlo (MC) modeling has predicted much lower physical dose enhancement with AuNPs at MV energies in which Compton effects, which have no relationship with Z , are dominant. For instance, Cho et al., predicted dose enhancement factors (DEFs) of 2.11 for 7 mg Au/g tumour with 140 kVp X-rays and 1.007 for 6 MV energies (Cho, 2005).

$$\text{DEF} = \frac{\text{Dose with Radiation Alone}}{\text{Dose with Radiation + AuNPs}}$$
 which produce the same biological effect

Where if the DEF is greater than one, then the addition of the drug is a radiosensitizer. If less than one, the drug acts as a radioprotector.

Another MC modeling simulation exploring the clinical applications of gold with different beam energies, suggested that using photon sources above the K-edge (80.7keV) of gold would require a higher gold concentration and is dependent on its location in the tumor region for a therapeutic effect (Lechtman et al., 2011), stressing the importance of AuNP uptake and location.

1.2.4 – AuNP delivery

The therapeutic impact of AuNPs or any pharmaceutical agent is dependent on the extent to which the drug penetrates tissue to reach its intended target. Passive approaches in AuNP delivery utilize the specific properties of tumour tissue such as abnormal angiogenesis and vascular leakage. These tumour blood vessels are irregularly shaped and are leaky which can facilitate the uptake of pharmaceutical agents or AuNPs to the targeted area; gaps as large as $2\mu\text{m}$ in diameter have been reported (McDonald & Baluk, 2002). This property is referred to as the enhanced permeability and retention (EPR) effect, where the gaps provide an entryway for molecules to enter into the blood inside the vessel of the tumour to permit more accumulation shown in Figure 1.2.

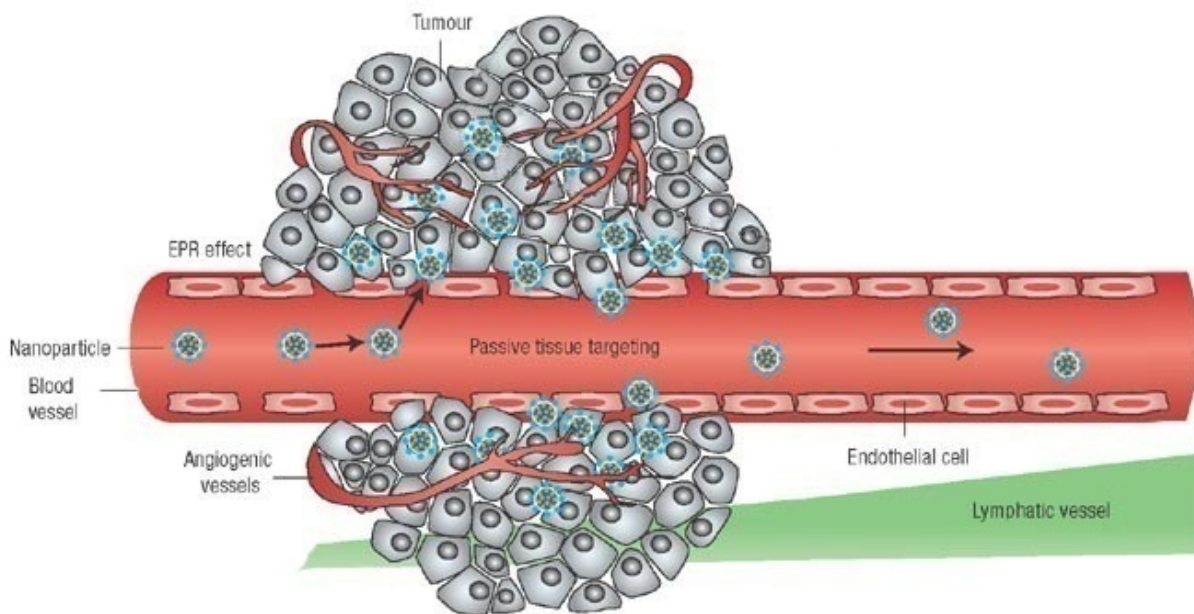


Figure 1.2: Enhanced permeability and retention effect. Nanoparticles are able to enter into the tumour region via leaky tumour vasculature, allowing local uptake (adapted from Peer et al., 2007).

The EPR effect with AuNPs have been shown *in vivo* to have preferentially uptake into tumours in mice and has led to improvements in tumour control following radiotherapy (Hainfeld et al., 2010; Kennedy et al., 2011; Zheng et al., 2008). The pioneer study done by Hainfeld et al., reported that through the administration of 1.9nm AuNPs prior to radiation, AuNPs could cause an increase in

tumour cell death. However, the amount of AuNPs administered to the mice was 1.35g/kg of Au, making the concentration impractical for human applications.

In order to decrease the amount administered to the patient and maintain a similar radiosensitization, the AuNPs should be targeted to the tumour cells. AuNPs added to plasmid DNA has been shown to increased damage to the plasmid by a factor of 2.5 compared to pure DNA, suggesting AuNPs should be close to maximize its effect on nuclear DNA (Zheng *et al.*, 2008). Clinical applications are mainly limited by the amount that can be administered to the patient and the method of preferentially retaining the AuNPs in cancer cells. Conversely, without an appropriate surface coating, nanoparticles in the blood stream are rapidly removed from circulation, limiting their availability for tumour uptake.

1.2.5– Increasing AuNP delivery

Although AuNPs are relatively inert, the surface of AuNPs is one of the most stable and easily functional platforms for molecular conjugation. AuNPs are usually coated in order to prevent opsonin proteins to bind and associate with macrophages, especially within the liver. This can result in AuNP accumulation within the liver and not to the targeted area. The addition of polyethylene glycol (PEG) has been shown to prevent opsonization resulting in a decrease in liver accumulation and increase in availability for therapy. PEG is used as a nontoxic, water-soluble stabilizer and has been found in a variety of products such as toothpaste, beauty products, and laxatives. It is the most common and preferred method in decreasing blood protein interaction and avoid immune recognition (Jokerst *et al.*, 2011; Zhang *et al.*, 2008). Covalently attached methoxy-PEG (mPEGs) of 1900 and 5000Da to bovine liver catalase was demonstrated to cause an increase in circulation time within the blood *in vivo* and resist digestion (Abuchowski *et al.*, 1977).

Other surface-modifying agents are used to increase AuNP delivery using a form of active transport and have been investigated in both *in vitro* and *in vivo* settings. Kennedy *et al.*, demonstrated that the

internalization of AuNP into activated human T-cells for delivery was achievable and increased delivery efficiency by four folds compared to freely injecting AuNPs (Kennedy, 2003). Liposomes carriers have also been shown to be a viable strategy for 1.4nm AuNP delivery, enhancing 1000 fold in cellular uptake (Chithrani et al., 2010). This project will explore an alternative, physical method of AuNP delivery.

1.3 – The physics of ultrasound

Ultrasound is a sound wave that is above the typical human audible range ($f \geq 20$ KHz). The transmitted pressure wave propagates in a medium through the oscillatory motion of particles. In longitudinal waves, commonly used to describe wave propagation in fluid and tissue media, the oscillation of particles are parallel to the wave propagation, creating regions of compression and rarefaction. During ultrasound propagation, due to different tissue densities, ultrasound waves interact with tissue, resulting in the scattering and absorption of energy. This property allows for the utilization of ultrasound in both imaging and therapeutic purposes.

1.3.1 – Ultrasound in imaging and therapy

Ultrasound energy is absorbed mostly in tissues with high collagen, allowing it to provide information on soft tissue structures and blood flow in vessel. In addition, acoustic characteristics such as tissue density and compressibility can be determined by different modes of imaging (Szabo, 2004). Ultrasound is a non-invasive form of guiding and monitoring invasive procedures in medicine. However, beyond traditional imaging, ultrasound has been known to produce biological effects depending on its exposure conditions (Feril & Kondo, 2004).

The absorption of ultrasonic energy at high intensities and high frequencies results in tissue heating and can be used for physical therapy to ablate tissue or locally release temperature sensitive drugs (Kennedy, 2003; Tacker & Anderson, 1982). At lower frequencies, its non-thermal effects may be posed as favourable for drug delivery, sonothrombolysis and gene therapy (Feril & Kondo, 2004) and is attributed to acoustically generated cavitation and radiation force. Radiation force is the pressure exerted in the direction of the ultrasound propagation. In acoustic cavitation, the propagated sound wave interacts with gas filled microbubbles. These microbubbles may be found in large liquid depositories within the body and are created by ultrasound. Microbubbles can also be introduced through injections into the body as contrast agents (O'Brien, 2007).

1.3.2 – Ultrasound and microbubbles

Microbubbles are currently used as ultrasound contrast agents (UCAs) due to their different echogenicity compared to tissue. These UCAs are approximately 1-8 μm in diameter and have a shell encapsulated gas core. The shell of the microbubble is usually composed of lipids, proteins and/or polymers ranging from 2-500nm in thickness (Hernot & Klibanov, 2008). Its gas core consists of gases of higher molecular weight in comparison to air, such as perfluorocarbon, nitrogen, or octafluoropropane for stability (Bull, 2007).

At relatively low acoustic pressures (mechanical index (MI) of < 0.2), the microbubbles undergo linear oscillations. The bubble vibrations produce ultrasound scattering with a frequency that is similar to the transmitted frequency. At higher acoustic pressures (MI of $0.2 - 0.5$), the bubble expansions and compression leads to non-linear oscillations and backscattering at multiple frequencies. This phenomenon is known as stable or non-inertial cavitation (Figure 1.3) where the various frequencies detected are from harmonic, sub-harmonic and ultra harmonics frequencies. The detection of these harmonic frequency signals has been implemented in ultrasound imaging equipment and have aided in enhancing the bubble-to-tissue backscatter signal ratio (Hernot & Klibanov, 2008).

At greater acoustic pressures ($MI > 0.5$), the forced expansion and compression of the microbubble frequently results in its destruction. The outward diffusion of gas during compression or fragmentation of the microbubble shell attribute to its collapse (Chomas *et al.*, 2001). The collapse of a microbubble is vital for quantifying perfusion with trigger imaging methods. Due to the rheological properties of microbubbles being similar to red blood cells, a continuous infusion of microbubbles within the body provides evaluation of myocardial replenishment rate and blood flow (Keller *et al.*, 1989).

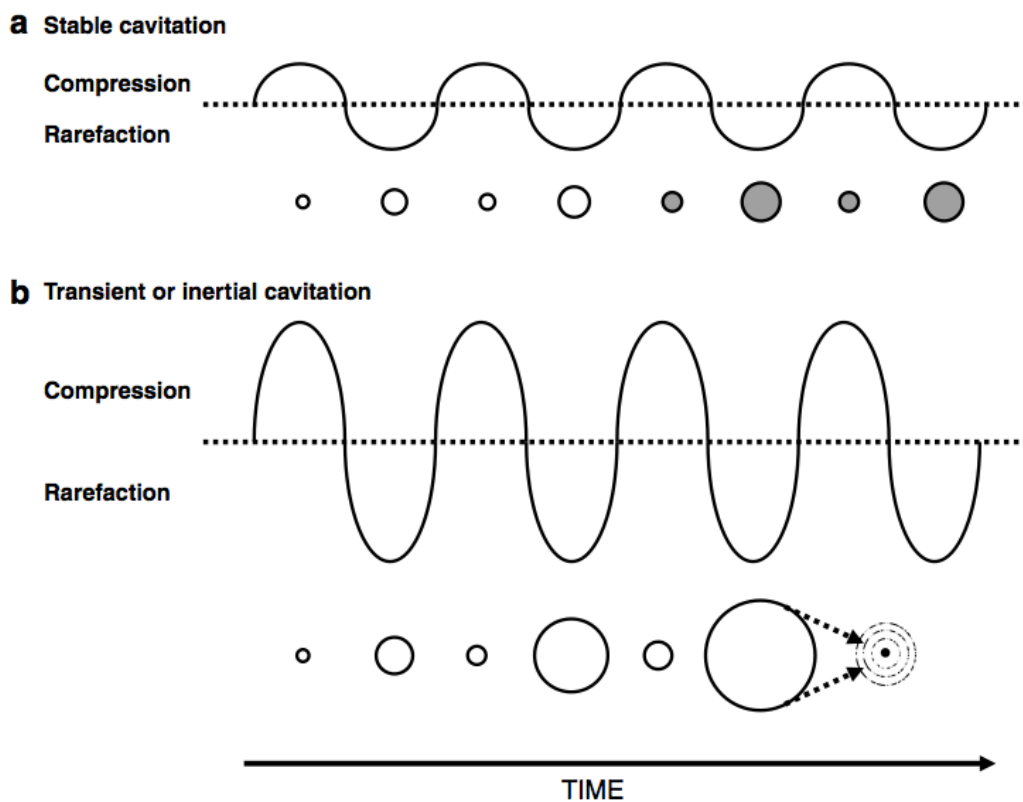


Figure 1.3: An illustration of a microbubble in an ultrasound field at a) low and b) high pressures. At low pressures, stable oscillation occurs (shaded circles) when its resonant, where at higher pressures, transient cavitation occurs when the inertial energy of the fluid surrounding the microbubble during compression causes the gas to diffuse out, forcibly collapsing the bubble (adapted from Newman & Bettinger, 2007).

UCAs have also been found to improve therapeutic efficacy in delivering pharmaceutical agents through loading microbubbles. The agent can be attached to the shell of the microbubble and

released upon ultrasound induced disruption (Hernot & Klivanov, 2008; Lentacker *et al.*, 2009). This method has also been introduced into gene therapy for encapsulating genetic material with the benefit of degradation prevention within the blood stream. In addition, microbubbles have been used to target cancerous tissue to further enhance drug delivery while minimizing the toxic effects of therapeutic agents (Stieger *et al.*, 2007). When microbubbles are within the region of interest, ultrasound exposure can cause microbubble disruption, locally releasing the drug (Hernot *et al.*, 2008).

Due to radiation pressure exerted on the bubble in the direction of the sound wave, the force can be used to direct microbubbles to the endothelial cells of vessel walls. Extravasation through blood vessels and receptor-ligand contact can increase the localization of the drug (Bull, 2007; Rychak *et al.*, 2007). The application of ultrasound and microbubbles to produce beneficial biological effects such as improving intracellular delivery is known as sonoporation.

1.3.3 – Sonoporation

Sonoporation is the event of transient and reversible pore formation that has been used to improve the delivery of therapeutic agents by increase cell permeability. Pores as large as 30-100nm were observed on ultrasound and microbubble treated cells from electron microscopy (Karshafian *et al.*, 2010; Zhou *et al.*, 2009). The pores were able to reseal within a few seconds to 24 hours (Zhou *et al.*, 2009). This allows the transport of usually non-permeable molecules to cross the cell membrane as shown in Figure 1.4. Sonoporation mediated drug and gene therapy is currently being developed to efficiently delivery drugs to challenging areas, non-invasively. This includes allowing pharmaceutical agents to cross the blood-brain barrier (Mears & Alonso, 2007), drugs for cardiovascular treatments (Schlicher *et al.*, 2006), and cancer therapeutic agents (Iwanaga *et al.*, 2007). Besides these advantageous effects of sonoporation, other undesired bioeffects may accompany cavitation. Membrane permeabilization with high pressures may result in cell death. To improve the therapeutic

ratio, increasing delivery of pharmaceutical agents through large amounts of pore, can cause cell death ultimately preventing delivery.

The success in determining the fine line between high permeability and high cell viability is dependent on the comprehension of microbubble behaviour within an ultrasound field and its mechanism of action during sonoporation.

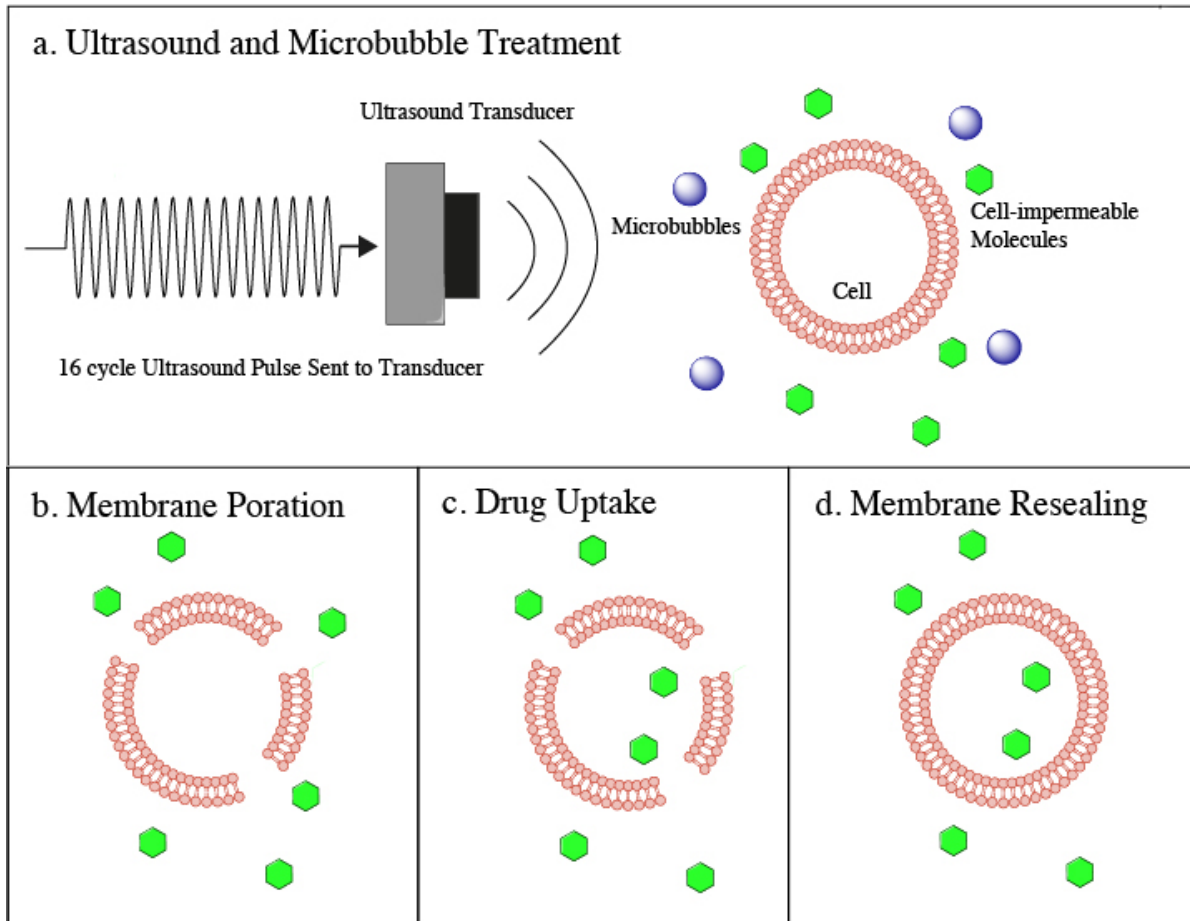


Figure 1.4: Schematic diagram of ultrasound and microbubble induced sonoporation where a) when microbubbles are placed in an ultrasound field, the microbubbles undergo oscillation causing the phenomenon known as sonoporation. This b) allows macromolecules to c) enter the intracellular matrix, eventually d) resealing.

1.3.4 – Mechanism of sonoporation

Although the mechanism of sonoporation remains unclear, a transient increase in the porosity and permeability of the cell membrane may be caused by the microbubble. The fate of the

microbubble is determined by: its environment, the size and shell of the bubble, and ultrasound parameters (Chen *et al.*, 2003; Karshafian, 2009). Microbubble distance between it and the cell have been demonstrated to influence cell permeability and resulting in a dependency on bubble-to-cell ratio. Cells closer in proximity were more likely to die during ultrasound exposure (Karshafian, 2009). Microbubbles are also influenced by its environment such as, surface tension, temperature, and viscosity of its surroundings (Liang *et al.*, 2009). In general, cell permeability increases along with acoustic pressure, until a threshold, which is then followed by a decrease in permeability (Karshafian, 2009; Liang *et al.*, 2009) and an increase in cell death. Cell death is more likely to occur with an increase in pulse duration, pulse repetition frequency, and insonation time. The optimal ultrasound parameters that demonstrated more cell permeability with the least amount of cell death was determined *in vitro* (Karshafian, 2009).

The acoustic mechanisms responsible for improving cellular uptake are the aforementioned stable and inertial (transient) cavitation. In stable cavitation, a microbubble will oscillate around an equilibrium radius when placed in an ultrasound field above its acoustic threshold. At the microbubbles resonant frequency, the microbubble undergo maximum oscillation. This stable oscillation causes strong liquid flow around the microbubble (microstreaming). Microbubbles oscillating in an ultrasound field creates a cyclical pressure field that creates eddy currents in the surrounding fluids. This may apply shear stress on nearby cell membranes (Feril & Kondo, 2004). In inertial cavitation, the microbubble drastic expansion is followed by a rapid violent collapse generating shockwaves with potential microjet formation. The likelihood and intensity of the collapse increases as ultrasound energy increase and frequency decreases. Due to the mechanical stress the microbubble has posed onto the membrane, intracellular deliveries of therapeutic agent are achievable (Blomley *et al.*, 2001; Hernot & Klibanov, 2008)

1.3.5 – Radiosensitization of ultrasound-microbubble and possible mechanism

Studies have indicated that endothelial cells undergo apoptosis when exposed to radiation, resulting in damaged tumour vasculature and secondary tumour cell death (Garcia-Barros *et al.*, 2003; Paris *et al.*, 2001). Microbubbles introduced *in vivo*, are injected into blood vessels, interacting with endothelial cells when exposed to an ultrasound field. Ultrasound mediated microbubble vasculature disruption has been shown to increase therapeutic effects of radiation when combined, inducing a 10 fold increase in cellular death at a dose of 2Gy with 160kVp (Czarnota *et al.*, 2012). In addition, the combined treatment of ultrasound and microbubble with radiation (USMB+XRT) exhibited a supraadditive effect *in vivo* compared to *in vitro*, implying a physiological mechanism involved in increasing tumour cell death. Vasculature damage has been confirmed to be dependent on ceramide, which is associated with inducing tumour cell death *in vivo* (Rotolo *et al.*, 2012). The confirmation of up regulated ceramide production post USMB+XRT was shown an *in vitro* cell suspension model where selected genes such as caspace9-alpha and caspace9-beta were activated with the combined treatment of USMB+XRT, but not USMB, or XRT alone (Al-Mahrouki *et al.*, 2012).

1.4 – Hypothesis

The proposed approach in increasing tumour cell death is to use ultrasound and microbubbles to increase AuNP uptake resulting in a localized dose enhancement when irradiated in cells. We have recently observed that ultrasound and microbubble-mediated (USMB) sonoporation can enhance radiation response *in vitro* and *in vivo* by the increased production of ceramide (Al-Mahrouki *et al.*, 2012; Czarnota *et al.*, 2012; Karshafian, 2009; Karshafian *et al.*, 2010). This will be the first study done with this combination.

The hypothesis driving this research is that ultrasound and microbubbles combined with gold nanoparticles can enhance radiotherapy. The specific objectives are to investigate the effect of the

combined treatment of USMB with AuNP on therapeutic outcome of radiotherapy, and to assess the effect of AuNP size and concentration and location on clonogenic cell viability.

1.5 - References

- Abuchowski, A., McCoy, J. R., Palczuk, N. C., van Es, T., & Davis, F. F. (1977). Effect of covalent attachment of polyethylene glycol on immunogenicity and circulating life of bovine liver catalase. *The Journal of Biological Chemistry*, 252(11), 3582–3586.
- Al-Mahrouki, A. A., Karshafian, R., Giles, A., & Czarnota, G. J. (2012). Bioeffects of Ultrasound-Stimulated Microbubbles on Endothelial Cells: Gene Expression Changes Associated with Radiation Enhancement in vitro. *Ultrasound in Medicine & Biology*. doi:10.1016/j.ultrasmedbio.2012.07.009
- Alkilany, A. M., Nagaria, P. K., Hexel, C. R., Shaw, T. J., Murphy, C. J., & Wyatt, M. D. (2009). Cellular Uptake and Cytotoxicity of Gold Nanorods: Molecular Origin of Cytotoxicity and Surface Effects. *Small*, 5(6), 701–708. doi:10.1002/smll.200801546
- Blomley, M. J., Cooke, J. C., Unger, E. C., Monaghan, M. J., & Cosgrove, D. O. (2001). Microbubble contrast agents: a new era in ultrasound. *BMJ (Clinical Research Ed.)*, 322(7296), 1222–1225.
- Bull, J. L. (2007). The application of microbubbles for targeted drug delivery. *Expert Opinion on Drug Delivery*, 4(5), 475–493. doi:10.1517/17425247.4.5.475
- Carter, J. D., Cheng, N. N., Qu, Y., Suarez, G. D., & Guo, T. (2007). Nanoscale energy deposition by X-ray absorbing nanostructures. *The Journal of Physical Chemistry B*, 111(40), 11622–11625. doi:10.1021/jp075253u
- Chattopadhyay, N., Cai, Z., Pignol, J.-P., Keller, B., Lechtman, E., Bendayan, R., & Reilly, R. M. (2010). Design and Characterization of HER-2-Targeted Gold Nanoparticles for Enhanced X-radiation Treatment of Locally Advanced Breast Cancer. *Molecular Pharmaceutics*, 7(6), 2194–2206. doi:10.1021/mp100207t
- Chen, W.-S., Brayman, A. A., Matula, T. J., & Crum, L. A. (2003). Inertial cavitation dose and hemolysis produced in vitro with or without Optison®. *Ultrasound in Medicine & Biology*, 29(5), 725–737. doi:10.1016/S0301-5629(03)00013-9
- Chithrani, B. D., Dunne, M., Stewart, J., Allen, C., & Jaffray, D. J. (2010). Cellular uptake and transport of gold nanoparticles incorporated in a liposomal carrier. *Nanomedicine: Nanotechnology, Biology, and Medicine*, 6(1), 161–169. doi:10.1016/j.nano.2009.04.009
- Chithrani, B. D., Ghazani, A. A., & Chan, W. C. W. (2006). Determining the Size and Shape Dependence of Gold Nanoparticle Uptake into Mammalian Cells. *Nano Letters*, 6(4), 662–668. doi:10.1021/nl052396o
- Cho, S. H. (2005). Estimation of tumour dose enhancement due to gold nanoparticles during typical radiation treatments: a preliminary Monte Carlo study. *Physics in Medicine and Biology*, 50(15),

N163–N173. doi:10.1088/0031-9155/50/15/N01

- Chomas, J. E., Dayton, P., Allen, J., Morgan, K., & Ferrara, K. W. (2001). Mechanisms of contrast agent destruction. *IEEE Transactions on Ultrasonics, Ferroelectrics, and Frequency Control*, *48*(1), 232–248.
- Czarnota, G. J. G., Karshafian, R. R., Burns, P. N. P., Wong, S. S., Al-Mahrouki, A. A., Lee, J. W. J., et al. (2012). Tumor radiation response enhancement by acoustical stimulation of the vasculature. *Pnas*, *109*(30), E2033–E2041. doi:10.1073/pnas.1200053109
- Dreaden, E. C., Mackey, M. A., Huang, X., Kang, B., & El-Sayed, M. A. (2011). Beating cancer in multiple ways using nanogold. *Chemical Society Reviews*, *40*(7), 3391. doi:10.1039/c0cs00180e
- Feril, L. B., Jr, & Kondo, T. (2004). Biological Effects of Low Intensity Ultrasound: The Mechanism Involved, and its Implications on Therapy and on Biosafety of Ultrasound. *Journal of Radiation Research*, *45*(4), 479–489. doi:10.1269/jrr.45.479
- Garcia-Barros, M., Paris, F., Cordon-Cardo, C., Lyden, D., Rafii, S., Haimovitz-Friedman, A., et al. (2003). Tumor response to radiotherapy regulated by endothelial cell apoptosis. *Science*, *300*(5622), 1155–1159. doi:10.1126/science.1082504
- Goorley, T., & Nikjoo, H. (2000). Electron and photon spectra for three gadolinium-based cancer therapy approaches. *Radiation Research*, *154*(5), 556–563. doi:10.1667/0033-7587(2000)154[0556:EAPSFT]2.0.CO;2
- Hainfeld, J. F., Dilmanian, F. A., Slatkin, D. N., & Smilowitz, H. M. (2008). Radiotherapy enhancement with gold nanoparticles. *Journal of Pharmacy and Pharmacology*, *60*(8), 977–985. doi:10.1211/jpp.60.8.0005
- Hainfeld, J. F., Dilmanian, F. A., Zhong, Z., Slatkin, D. N., Kalef-Ezra, J. A., & Smilowitz, H. M. (2010). Gold nanoparticles enhance the radiation therapy of a murine squamous cell carcinoma. *Physics in Medicine and Biology*, *55*(11), 3045–3059. doi:10.1088/0031-9155/55/11/004
- Hainfeld, J. F., Slatkin, D. N., & Smilowitz, H. M. (2004). The use of gold nanoparticles to enhance radiotherapy in mice. *Physics in Medicine and Biology*, *49*(18), N309–N315. doi:10.1088/0031-9155/49/18/N03
- Hainfeld, J. F., Slatkin, D. N., Focella, T. M., & Smilowitz, H. M. (2006). Gold nanoparticles: a new X-ray contrast agent. *British Journal of Radiology*, *79*(939), 248–253. doi:10.1259/bjr/13169882
- Hauck, T. S., Ghazani, A. A., & Chan, W. C. W. (2008). Assessing the Effect of Surface Chemistry on Gold Nanorod Uptake, Toxicity, and Gene Expression in Mammalian Cells. *Small*, *4*(1), 153–159. doi:10.1002/smll.200700217
- Hernot, S., & Klibanov, A. L. (2008). Microbubbles in ultrasound-triggered drug and gene delivery.

- Advanced Drug Delivery Reviews*, 60(10), 1153–1166. doi:10.1016/j.addr.2008.03.005
- Huang, X., & El-Sayed, M. A. (2010). Gold nanoparticles: Optical properties and implementations in cancer diagnosis and photothermal therapy. *Journal of Advanced Research*, 1(1), 13–28. doi:10.1016/j.jare.2010.02.002
- Iwanaga, K. K., Tominaga, K. K., Yamamoto, K. K., Habu, M. M., Maeda, H. H., Akifusa, S. S., et al. (2007). Local delivery system of cytotoxic agents to tumors by focused sonoporation. *Cancer Gene Therapy*, 14(4), 354–363. doi:10.1038/sj.cgt.7701026
- Jain, S., Coulter, J. A., Hounsell, A. R., Butterworth, K. T., McMahon, S. J., Hyland, W. B., et al. (2011). Cell-specific radiosensitization by gold nanoparticles at megavoltage radiation energies. *International Journal of Radiation Oncology, Biology, Physics*, 79(2), 531–539. doi:10.1016/j.ijrobp.2010.08.044
- Jokerst, J. V., Lobovkina, T., Zare, R. N., & Gambhir, S. S. (2011). Nanoparticle PEGylation for imaging and therapy. *Nanomedicine*, 6(4), 715–728. doi:10.2217/nnm.11.19
- Karshafian, R. (2009). On the Permeabilisation and Disruption of Cell Membranes by Ultrasound and Microbubbles, 1–123.
- Karshafian, R., & Tchouala, J. I. N. (2010). Enhancement of Radiation Therapy by Ultrasonically-stimulated Microbubbles In Vitro: Effects of Treatment Scheduling on Cell Viability and Production of Ceramide. *Ultrasonics Symposium (IUS)*, 2010, 2115–2118. doi:10.1109/ULTSYM.2010.0534
- Karshafian, R., Bevan, P. D., Williams, R., Samac, S., & Burns, P. N. (2009). Sonoporation by Ultrasound-Activated Microbubble Contrast Agents: Effect of Acoustic Exposure Parameters on Cell Membrane Permeability and Cell Viability. *UMB*, 35(5), 847–860. doi:10.1016/j.ultrasmedbio.2008.10.013
- Karshafian, R., Samac, S., Bevan, P. D., & Burns, P. N. (2010). Microbubble mediated sonoporation of cells in suspension: Clonogenic viability and influence of molecular size on uptake. *Ultrasonics*, 50(7), 691–697. doi:10.1016/j.ultras.2010.01.009
- Keller, M. W., Segal, S. S., Kaul, S., & Duling, B. (1989). The behavior of sonicated albumin microbubbles within the microcirculation: a basis for their use during myocardial contrast echocardiography. *Circulation Research*, 65(2), 458–467.
- Kennedy, J. E. (2003). High intensity focused ultrasound: surgery of the future? *British Journal of Radiology*, 76(909), 590–599. doi:10.1259/bjr/17150274
- Kennedy, L. C., Bear, A. S., Young, J. K., Lewinski, N. A., Kim, J., Foster, A. E., & Drezek, R. A. (2011). T cells enhance gold nanoparticle delivery to tumors in vivo. *Nanoscale Research Letters*, 6(1), 283. doi:10.1186/1556-276X-6-283

- Kinsella, T. J., Schupp, J. E., Davis, T. W., Berry, S. E., Hwang, H. S., Warren, K., et al. (2000). Preclinical study of the systemic toxicity and pharmacokinetics of 5-iodo-2-deoxypyrimidinone-2'-deoxyribose as a radiosensitizing prodrug in two, non-rodent animal species: implications for phase I study design. *Clinical Cancer Research*, 6(9), 3670–3679.
- Kong, T., Zeng, J., Wang, X., Yang, X., Yang, J., McQuarrie, S., et al. (2008). Enhancement of Radiation Cytotoxicity in Breast-Cancer Cells by Localized Attachment of Gold Nanoparticles. *Small*, 4(9), 1537–1543. doi:10.1002/sml.200700794
- Lechtman, E., Chattopadhyay, N., Cai, Z., Mashouf, S., Reilly, R., & Pignol, J. P. (2011). Implications on clinical scenario of gold nanoparticle radiosensitization in regards to photon energy, nanoparticle size, concentration and location. *Physics in Medicine and Biology*, 56(15), 4631–4647. doi:10.1088/0031-9155/56/15/001
- Lentacker, I., De Smedt, S. C., & Sanders, N. N. (2009). Drug loaded microbubble design for ultrasound triggered delivery. *Soft Matter*, 5(11), 2161. doi:10.1039/b823051j
- Liang, H.-D., Tang, J., Halliwell, M., & Wells, P. N. T. (2009). Sonoporation, drug delivery, and gene therapy. *Proceedings of the Institution of Mechanical Engineers, Part H: Journal of Engineering in Medicine*, 224(2), 343–361. doi:10.1243/09544119JEM565
- Matsudaira, H., Ueno, A. M., & Furuno, I. (1980). Iodine contrast medium sensitizes cultured mammalian cells to X rays but not to gamma rays. *Radiation Research*, 84(1), 144–148.
- McDonald, D. M., & Baluk, P. (2002). Significance of blood vessel leakiness in cancer. (Vol. 62, pp. 5381–5385). Presented at the Cancer research.
- McMahon, S. J., Mendenhall, M. H., Jain, S., & Currell, F. (2008). Radiotherapy in the presence of contrast agents: a general figure of merit and its application to gold nanoparticles. *Physics in Medicine and Biology*, 53(20), 5635–5651. doi:10.1088/0031-9155/53/20/005
- Meairs, S., & Alonso, A. (2007). Ultrasound, microbubbles and the blood-brain barrier. *Progress in Biophysics and Molecular Biology*, 93(1-3), 354–362. doi:10.1016/j.pbiomolbio.2006.07.019
- Mello, R. R. S., Callisen, H. H., Winter, J. J., Kagan, A. R. A., & Norman, A. A. (1983). Radiation dose enhancement in tumors with iodine. *Medical Physics*, 10(1), 75–78.
- Mesbahi, A. (2010). A review on gold nanoparticles radiosensitization effect in radiation therapy of cancer. *Reports of Practical Oncology & Radiotherapy*, 15(6), 176–180. doi:10.1016/j.rpor.2010.09.001
- Nath, R., Bongiorno, P., & Rockwell, S. (1990). Iododeoxyuridine radiosensitization by low- and high-energy photons for brachytherapy dose rates. *Radiation Research*, 124(3), 249–258.
- Newman, C. M. H. C., & Bettinger, T. T. (2007). Gene therapy progress and prospects: ultrasound for

- gene transfer. *Gene Therapy*, 14(6), 465–475. doi:10.1038/sj.gt.3302925
- O'Brien, W. D. J. (2007). Ultrasound-biophysics mechanisms (Vol. 93, pp. 212–255). Presented at the Progress in Biophysics & Molecular Biology. doi:10.1016/j.pbiomolbio.2006.07.010
- Pan, Y., Neuss, S., Leifert, A., Fischler, M., Wen, F., Simon, U., et al. (2007). Size-dependent cytotoxicity of gold nanoparticles. *Small*, 3(11), 1941–1949. doi:10.1002/sml.200700378
- Paris, F. F., Fuks, Z. Z., Kang, A. A., Capodiceci, P. P., Juan, G. G., Ehleiter, D. D., et al. (2001). Endothelial apoptosis as the primary lesion initiating intestinal radiation damage in mice. *Science*, 293(5528), 293–297. doi:10.1126/science.1060191
- Peer, D., Karp, J. M., Hong, S., Farokhzad, O. C., Margalit, R., & Langer, R. (2007). Nanocarriers as an emerging platform for cancer therapy. *Nature Nanotechnology*, 2(12), 751–760. doi:10.1038/nnano.2007.387
- Pignol, J.-P., Rakovitch, E., Beachey, D., & Le Sech, C. (2003). Clinical significance of atomic inner shell ionization (ISI) and Auger cascade for radiosensitization using IUdR, BUdR, platinum salts, or gadolinium porphyrin compounds. *International Journal of Radiation Oncology, Biology, Physics*, 55(4), 1082–1091.
- Polf, J. C., Bronk, L. F., Driessen, W. H. P., Arap, W., Pasqualini, R., & Gillin, M. (2011). Enhanced relative biological effectiveness of proton radiotherapy in tumor cells with internalized gold nanoparticles. *Applied Physics Letters*, 98(19), 193702. doi:10.1063/1.3589914
- Popovtzer, R., Agrawal, A., Kotov, N. A., Popovtzer, A., Balter, J., Carey, T. E., & Kopelman, R. (2008). Targeted Gold Nanoparticles Enable Molecular CT Imaging of Cancer. *Nano Letters*, 8(12), 4593–4596. doi:10.1021/nl8029114
- Robar, J. (2006). Generation and modelling of megavoltage photon beams for contrast-enhanced radiation therapy. *Physics in Medicine and Biology*, 51, 5487–5504. doi:10.1088/0031-9155/51/21/007
- Rotolo, J. J., Stancevic, B. B., Zhang, J. J., Hua, G. G., Fuller, J. J., Yin, X. X., et al. (2012). Anti-ceramide antibody prevents the radiation gastrointestinal syndrome in mice. *Journal of Clinical Investigation*, 122(5), 1786–1790. doi:10.1172/JCI59920
- Rychak, J. J., Klivanov, A. L., Ley, K. F., & Hossack, J. A. (2007). Enhanced targeting of ultrasound contrast agents using acoustic radiation force. *Ultrasound in Medicine & Biology*, 33(7), 1132–1139. doi:10.1016/j.ultrasmedbio.2007.01.005
- Schlicher, R. K., Radhakrishna, H., Tolentino, T. P., Apkarian, R. P., Zarnitsyn, V., & Prausnitz, M. R. (2006). Mechanism of intracellular delivery by acoustic cavitation. *Ultrasound in Medicine & Biology*, 32(6), 915–924. doi:10.1016/j.ultrasmedbio.2006.02.1416

- Stieger, S. M., Caskey, C. F., Adamson, R. H., Qin, S., Curry, F. R. E., Wisner, E. R., & Ferrara, K. W. (2007). Enhancement of Vascular Permeability with Low-Frequency Contrast-enhanced Ultrasound in the Chorioallantoic Membrane Model. *Radiology*, 243(1), 112–121. doi:10.1148/radiol.2431060167
- Szabo, T. L. (2004). *Diagnostic Ultrasound Imaging: Inside Out - Thomas L. Szabo*. Elsevier Academic Press.
- Tacker, J. R., & Anderson, R. U. (1982). Delivery of antitumor drug to bladder cancer by use of phase transition liposomes and hyperthermia. *The Journal of Urology*, 127(6):1211-4.
- Tarapacki, C., Kumaradas, J. C., & Karshafian, R. (2012). Enhancing laser thermal-therapy using ultrasound-microbubble and gold nanorods of in vitro cells. *Ultrasonics*. doi:10.1016/j.ultras.2012.11.006
- Trono, J. D., Mizuno, K., Yusa, N., Matsukawa, T., Yokoyama, K., & Uesaka, M. (2011). Size, Concentration and Incubation Time Dependence of Gold Nanoparticle Uptake into Pancreas Cancer Cells and its Future Application to X-ray Drug Delivery System. *Journal of Radiation Research*, 52(1), 103–109. doi:10.1269/jrr.10068
- Webb, S. (2003). The physical basis of IMRT and inverse planning. *British Journal of Radiology*, 76(910), 678–689. doi:10.1259/bjr/65676879
- Yih, T. C., & Wei, C. (2005). Nanomedicine in cancer treatment. *Nanomedicine: Nanotechnology, Biology, and Medicine*, 1(2), 191–192. doi:10.1016/j.nano.2005.04.001
- Yu, C. X., & Tang, G. (2011). Intensity-modulated arc therapy: principles, technologies and clinical implementation. *Physics in Medicine and Biology*, 56(5), R31–54. doi:10.1088/0031-9155/56/5/R01
- Zhang, X., Xing, J. Z., Chen, J., Ko, L., Amanie, J., Gulavita, S., et al. (2008). Enhanced radiation sensitivity in prostate cancer by gold-nanoparticles (Vol. 31, pp. E160–E167). Presented at the Clinical and Investigative Medicine.
- Zheng, Y. Y., Hunting, D. J. D., Ayotte, P. P., & Sanche, L. L. (2008). Radiosensitization of DNA by gold nanoparticles irradiated with high-energy electrons. *Radiation Research*, 169(1), 19–27. doi:10.1667/RR1080.1
- Zhou, Y., Kumon, R. E., Cui, J., & Deng, C. X. (2009). The Size of Sonoporation Pores on the Cell Membrane. *Umb*, 35(10), 1756–1760. doi:10.1016/j.ultrasmedbio.2009.05.012

Chapter 2

IN VITRO STUDY

This chapter will be submitted to a peer-reviewed journal and includes an abstract and introduction.

Abstract

Purpose: Gold nanoparticles (AuNPs) have been shown to enhance the local radiation dose *in vitro* and *in vivo* due to its high Z value. Challenges arise when delivering AuNPs into the tumour.

Microbubbles in an ultrasound field at therapeutic conditions can increase the permeability of the phospholipid membrane and allow therapeutic agents to cross the bilayer. In this study, the AuNPs potential increase in uptake with ultrasound and microbubbles (USMB) will be investigated *in vitro*.

Materials and Methods: A cell suspension model using breast cancer (MDA MB 231) cells were exposed to USMB, 12 nm gold spheres or 12 x 44nm rods, and radiation. Gold at concentrations of 7.8×10^{10} nps/mL and 1.6×10^{11} nps/mL were investigated with USMB parameters of 500kHz pulse center frequency, 570kPa peak negative pressure, 10 μ s pulse duration, 60s insonation time, Definity microbubbles at 3.3% (v/v) and irradiation of 2Gy at 160kVp. Cell viability post treatment was evaluated with clonogenic assay.

Results: The results suggest that the combined treatment of AuNPs, and USMB aid in its delivery to increase cell death upon irradiation. An improvement of ~ 22 folds was observed with the combined treatment compared to radiation only. The combined treatment cell viability was ~3-4% depending and is dependent on AuNP concentration, shape and location.

Conclusion: With the addition of USMB to aid in the delivery of AuNPs, the results suggest a synergistic effect in cell death. Further investigation of this concept will be done *in vivo*.

Keywords: *Ultrasound therapy, Sonoporation, ultrasound-microbubble delivery, gold nano-particles, radiotherapy, radio-enhancement*

2.1 – Introduction

The therapeutic effect of radiotherapy has been shown to improve with gold nanoparticles (AuNPs) by ~ 3 or less (Kong *et al.*, 2008; Zhang *et al.*, 2008), which can potentially aid in the targeting of ionizing radiation. Delivery of AuNPs to cancerous tissues can be achieved through endocytosis *in vitro* (Chithrani *et al.*, 2006; Trono *et al.*, 2011) and the enhanced permeability and retention effect (EPR effect) to be preferentially taken up into tumours in mice and has led to improvements in tumour control following radiotherapy *in vivo* (Hainfeld *et al.*, 2008; Kennedy *et al.*, 2011). Although AuNP uptake is dependent on size, shape, and concentration (Chithrani *et al.*, 2010; Pan *et al.*, 2007; Trono *et al.*, 2011), poor AuNPs delivery can be addressed through coating, biological targeting, and most recently, ultrasound and microbubble mediated sonoporation (Tarapacki *et al.*, 2012; Chattopadhyay *et al.*, 2010; Hauck *et al.*, 2008) .

Gold nanoparticles (AuNPs) have been investigated as a radiosensitizing agent due to its high atomic number and relatively inert nature. Upon irradiation, the photoelectric effect in gold dominates and the photon energy is used to eject inner atomic shell electrons. The atomic shell reorganization, known as an Auger cascade, generates the emission of a localized dose of radiation at the microscopic scale (Pignol *et al.*, 2003). These characteristics of AuNP have made them a potential viable radiosensitizing agent in radiotherapy (Hainfeld *et al.*, 2006; Popovtzer *et al.*, 2008).

The hydrophobic nature of the semi-permeable lipid bilayer of a cell membrane prevents large molecules to diffuse across. AuNPs can be manufactured at various sizes and shapes, and conjugated with biological molecules to maximize delivery to biological tissues including cells. Many studies have shown that AuNP accumulation *in vitro* is primarily due to endocytosis and its non-specific absorption of AuNPs and are important for maximal intracellular uptake (Chithrani *et al.*, 2006; Pan *et al.*, 2007; Trono *et al.*, 2011). AuNPs stabilized by triphenylphosphine derivative in a variety of cell type, have been shown to be dependent primarily on size and not on ligand chemistry. Particles of 1-2nm in

diameter were determined to be toxic *in vitro*, where AuNPs of greater size were comparatively non-toxic (Pan *et al.*, 2007). The shape and size which provides maximum nanoparticle per cell is spherical 50nm AuNPs, ultimately reaching a plateau with increased concentrations at 20 μM (Chithrani *et al.*, 2006). However this may be dependent on cell line, since a plateau was not observed at concentrations of 94 μM (Trono *et al.*, 2011).

Challenges arise when delivering AuNPs to the target with optimal efficiency. When AuNPs are delivered via intravenous injections, the biodistribution of AuNP greatly resides within the bloodstream compared to the tumour and tumour peripheries post 5 minutes injection (Hainfeld *et al.*, 2004). In addition, Hainfeld suggests that higher concentrations of gold exhibit a greater radioenhancement (Hainfeld *et al.*, 2004). In an *in vitro* model, natural uptake of AuNPs through endocytosis was determined to be dependent on size and shape (Chithrani *et al.*, 2006). To be able to enhance the delivery of gold nanoparticles and determine AuNP characteristics that may affect the enhanced therapeutic effects of AuNP and radiations, combined, will provide a further understanding of its potential to aid in optimizing treatment parameters prior to its application in the clinic.

Microbubbles are currently used as ultrasound contrast agents (UCAs) due to its different echogenicity compared to tissue. However, traditionally used as a diagnostic tool, ultrasound and microbubbles are able to produce beneficial biological effects depending on exposure conditions (Feril & Kondo, 2004). When a microbubble is subjected to an ultrasound field of pressures above a particular amplitude threshold, the bubble will undergo oscillation or disruption. The fate of the microbubble is determined by: its environment, the size and shell of the bubble, and ultrasound parameters (Chen *et al.*, 2003; Karshafian *et al.*, 2009) and can cause a phenomenon known as *sonoporation* to occur. Sonoporation is the event of transient and reversible pore formation that has been used to improve the delivery of therapeutic agents by increasing cell permeability.

The acoustic mechanisms responsible for improving uptake are stable and inertial (transient)

cavitation. In stable cavitation, a microbubble will oscillate around an equilibrium radius when placed in an ultrasound field above its acoustic threshold. This stable oscillation causes strong liquid flow around the microbubble and may apply shear stress on nearby cell membranes (Feril & Kondo, 2004). In inertial cavitation, the microbubble drastic expansion is followed by a rapid violent collapse generating shockwaves with potential microjet formation. Due to the mechanical stress the microbubble has posed onto the membrane, intracellular deliveries of therapeutic agent are achievable (Blomley *et al.*, 2001; Hernot & Klibanov, 2008).

The proposed approach in increasing tumour cell death is to use ultrasound and microbubbles, to increase AuNP uptake resulting in a localized dose enhancement when irradiated in cells. We have recently observed that ultrasound and microbubble-mediated (USMB) sonoporation can enhance radiation response *in vitro* and *in vivo* by the increased production of ceramide (Al-Mahrouki *et al.*, 2012; Czarnota *et al.*, 2012; Karshafian, 2009; Karshafian *et al.*, 2010). This will be the first study done with this combination.

The hypothesis driving this research is that ultrasound and microbubbles combined with gold nanoparticles can enhance radiotherapy. The specific objectives are to investigate the effect of the combined treatment of USMB with AuNP on therapeutic outcome of radiotherapy, and to assess the effect of AuNP size and concentration and location on clonogenic cell viability.

2.2 – Materials and Methods: in vitro cell suspension

Cells in suspension were treated with AuNP, USMB, and radiotherapy and with combined treatments at varying AuNP characteristics. Cell viability was then assessed using clonogenic assay.

2.2.1 - In vitro cell model

A human adenocarcinoma breast cell line (MDA-MB-231) from the American Type Culture Collections (ATCC, MD, USA) was cultured in RPMI-1640 medium supplemented with 5%

penicillin/streptomycin antibiotic and 10% fetal bovine serum. The cells were incubated at 37°C and 5% CO₂ concentration and allowed to reach confluency. Cells were washed with Dulbecco's Phosphate Buffered Saline (DPBS), trypsinized and suspended in media. Prior to treatment, cells were prepared at a concentration of 1.5 million cells per mL and volume of 3 mL.

2.2.2 – Gold nanoparticles (AuNP)

Two AuNP sizes and concentrations (number of AuNP per mL) were used in this study. Gold nanoparticle spheres of 12nm (no CTAB content) and rods of 44nm by 12nm (CTAB < 10nM), (Nanopartz™, Inc., Loveland, CO, USA) were added to the cell suspension. Dilutions of AuNP 5.1 x 10¹¹ nps/mL were prepared with Milli-Q water. The concentrations of AuNP used were 7.8 x 10¹⁰ nps/mL and 1.6 x 10¹¹ nps/mL corresponding to 60nM and 116nM for spherically shaped AuNPs, and to 152nM and 320nM for rod-shaped AuNPs, respectively.

2.2.3 - Ultrasound and microbubble treatment

Cells were placed in an acoustic chamber and exposed to ultrasound pulses in the presence of a microbubble agent. The ultrasound exposure system consisted of a single element transducer of 500 kHz center-frequency (IL0509HP, Valpey Fisher Inc., Hopkinton, MA) mounted to a micro-positioning system, a waveform generator (AWG520, Tektronix Inc., Beaverton, OR) and a power amplifier (RPR4000, Ritec Inc., Warwick, RI). The cell exposure chamber was of cylindrical shape with 12 mm internal diameter and 10 mm diameter through hole across the cylinder, with Mylar membranes glued on both sides with a magnetic stirrer within the chamber. The cell suspension was placed in the exposure chamber along with AuNPs and microbubbles and then exposed to ultrasound pulses at 32 μs pulse duration, 1kHz pulse repetition frequency, and 60s insonation time at 570kPa negative peak pressure based on previous sonoporation experiments (Karshafian, 2009). Definity® (Lantheus Medical Imaging, Inc., North Billerica, MA, USA) microbubbles, a clinically approved agent, at a concentration of 3.3% v/v (volume concentration) was used. The microbubbles were prepared by activating the Definity® vial using a Vialmix® (Lantheus Medical Imaging, Inc., North Billerica, MA, USA) for 45

seconds. The agent was allowed to reach room temperature prior to activation. According to the manufacturer, the mean diameter range of the generated microspheres was 1.1 μ m to 3.3 μ m, and the maximum diameter was 20 μ m.

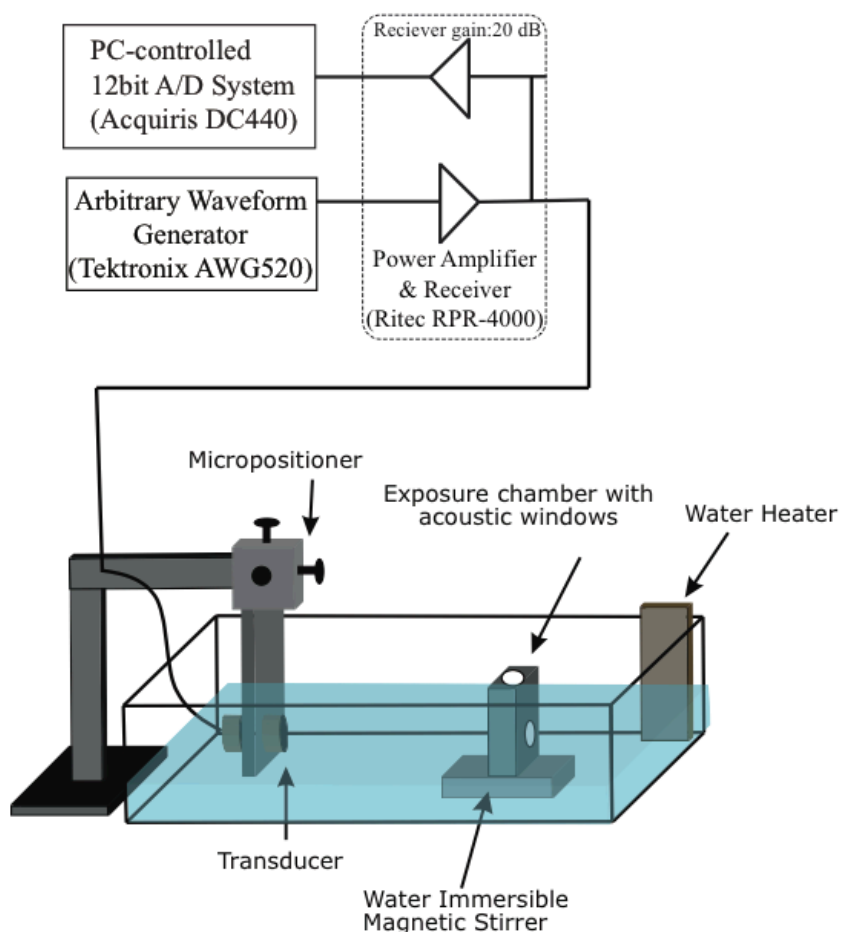


Figure 2.1: A schematic diagram of the ultrasound exposure apparatus. Cells are placed within the chamber and exposed to set acoustic conditions (Reprinted from Karshafian *et al.*, 2009)

2.2.4 – Radiotherapy (XRT)

Cells were exposed to ionizing radiation either following centrifugation of the cell suspension (to remove the AuNP from the solution) or without (with AuNP remaining in the supernatant of the cell suspension). The cells were then transferred to 35mm petri dishes and irradiated with 2Gy single fraction dose at 160kVp and 200cGy/min dose rate (Faxitron X-ray Corporation, Lincolnshire, IL, USA).

2.2.5 – Clonogenic assay

Following the combined treatment of AuNP, USMB and XRT, cell viability was assessed using clonogenic assay (denoted by V_C). Cells were plated in 50mm culture dishes and incubated for 13-15 days. The cells were stained with Methylene blue and counted using a microscope. Experiments were repeated with four independent samples, and colony assay were done in triplicate (n=12).

2.2.6 – Analysis

Synergism of the combined treatment was assessed using the Bliss independence criterion (Bliss, 2008), where the expected additive effect on cell viability (V_A) for the combined therapy was compared to experimental measurements. The expected additive response of the combined treatments was calculated based on the measured cell viability (V_C) of each treatment. The combined treatment was considered synergistic when V_C was statistically lower than V_A . A Tukey post-hoc was done to compare each treatment and determined its significance. V_A and V_C were compared with a non parametric T-test.

2.3 – Results

Ultrasound and microbubbles in combination with gold nanoparticles synergistically improved therapeutic response of radiotherapy. Cell viability decreased by ~22 fold with spherical shaped AuNP+USMB+XRT ($V_C = 3\%$) compared to XRT alone ($V_C = 65\%$) and by ~11 fold compared to AuNP+XRT ($V_C = 34\%$). The effectiveness of the combined treatment depended on AuNP characteristics and the location of the AuNP in the intracellular and extracellular space.

2.3.1 – AuNP Spheres with USMB and XRT

Clonogenic viability of cells treated with USMB, XRT and AuNP with spherical (12nm) and rod-shaped (12nm by 44 nm) are shown in Figures 2.2 and 2.3, respectively; (a) and (b) represents samples without AuNPs in solution (centrifuged samples) and with AuNPs in solution (non-centrifuged samples), respectively. The lowest cell viability was achieved with the combined treatment of AuNP+USMB+XRT ($V_C = 3\%$) at the higher AuNP concentration (1.6×10^{11} nps/mL). A maximum of ~22 fold decrease was achieved in cell viability with the combined treatment compared with XRT alone (Figure 2.2a). At the higher AuNP concentration, cell viability was statistically lower with the combined treatment ($V_C = 3\%$) compared to USMB+XRT ($V_C = 18\%$), whereas at the lower AuNP concentration no statistically significant difference was observed ($V_C = 14\%$).

Spherical AuNPs improved therapeutic response of XRT by ~2 fold with AuNPs in solution. V_C of 65% was achieved with XRT alone compared to 34% with AuNP+XRT at both concentrations of AuNP (7.8×10^{10} nps/mL and 1.6×10^{11} nps/mL) (Figure 2.2a). No statistically significant difference was observed with AuNP alone compared to untreated control, although on average cell viability decreased by 8%. Whereas, viability of cells treated with AuNP+USMB decreased by ~1.5 fold, corresponding to 20% decreased in V_C , compared to USMB alone at both AuNP concentrations (Figure 2.2a). In addition, USMB treatment improved therapeutic response of XRT, as expected. V_C of 18% was

observed with USMB+XRT, which was significantly lower compared to XRT alone ($V_C = 65\%$) and USMB alone ($V_C = 58\%$).

Furthermore, the presence of AuNP spheres in the solution of the cell suspension decreased cell viability. Cell viability of samples treated with USMB and XRT in the presence of AuNP in solution were generally lower by ~2-6 fold (Figure 2.2b) compared to samples without AuNP in solution (Figure 2.2a). In XRT treated samples, the presence of AuNP spheres in solution decreased cell viability by ~10%; V_C of 34% and 25% was observed with AuNP+XRT treatment without and with AuNP in the solution.

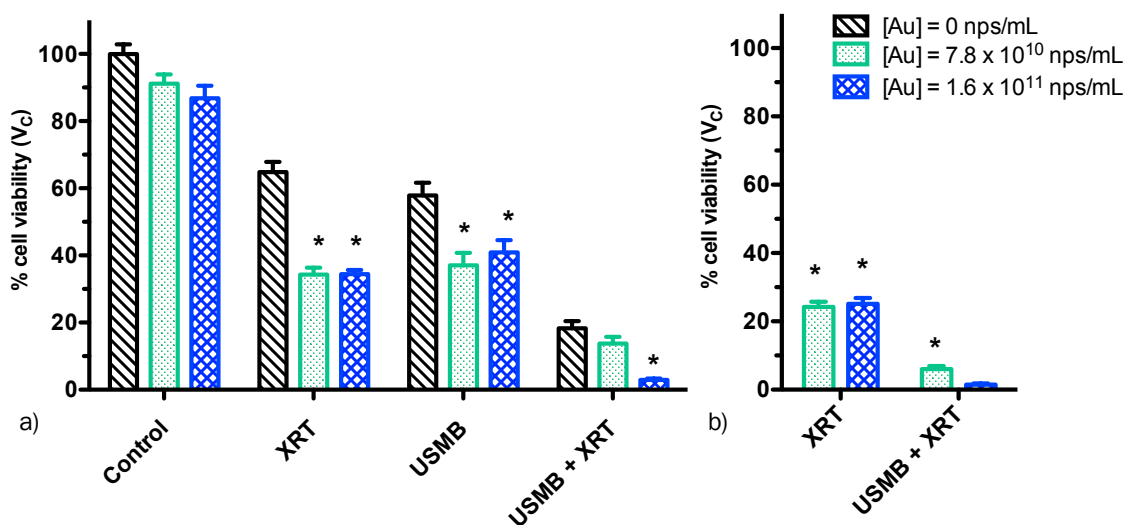


Figure 2.2: Clonogenic viability of MDA-MB231 cells exposed to 12nm AuNP spheres were normalized to the control. a) Two different concentrations of AuNP, USMB fixed at 0.5MHz frequency pulses with 570kPa negative peak pressure and 3.3% (v/v) microbubbles, and a 160kVp 2Gy single radiation dose and their combinations are shown. The asterisks signify its statistical significance in comparison to samples without AuNPs, 0 nps/mL concentration. These samples were centrifuged, removing gold within the solution before irradiation. Cell viability of AuNP, USMB, and XRT combined treatments with gold in solution is represented in b). The asterisks in Figure 2.2b) represents its statistical significance ($P < 0.05$) compared with its corresponding condition in Figure 2.2a).

2.3.2 – AuNP Rods with USMB and XRT

The combined treatment of USMB and rod-shaped AuNP at the higher concentration also improved the therapeutic response of XRT by ~16 folds (Figure 2.3a); V_C of 4% was achieved with rod-

shaped AuNP+USMB+XRT. The rod-shaped AuNPs appeared to have similar effect compared to spherical-shaped AuNPs. At the higher AuNP concentration, cell viability of ($V_C = 20\%$) with AuNP+XRT compared to AuNP alone ($V_C = 42\%$) and XRT alone ($V_C=63\%$) were achieved. USMB decreased cell viability by 45%, and in combination with rod-shaped AuNP cell viability was further decreased by 14% to 26%. However, the presence of the AuNP rods in the cell suspension induced a more pronounced effect on cell viability compared to AuNP spheres (Figures 2.2a and 2.3a). In addition, the presence of the rod-shaped AuNPs in solution during XRT treatment further decreased cell viability. V_C of 22% and 49% were achieved with AuNP+XRT when AuNPs were present and absent from the solution of the cell suspension (7.8×10^{10} nps/mL) (Figure 2.3).

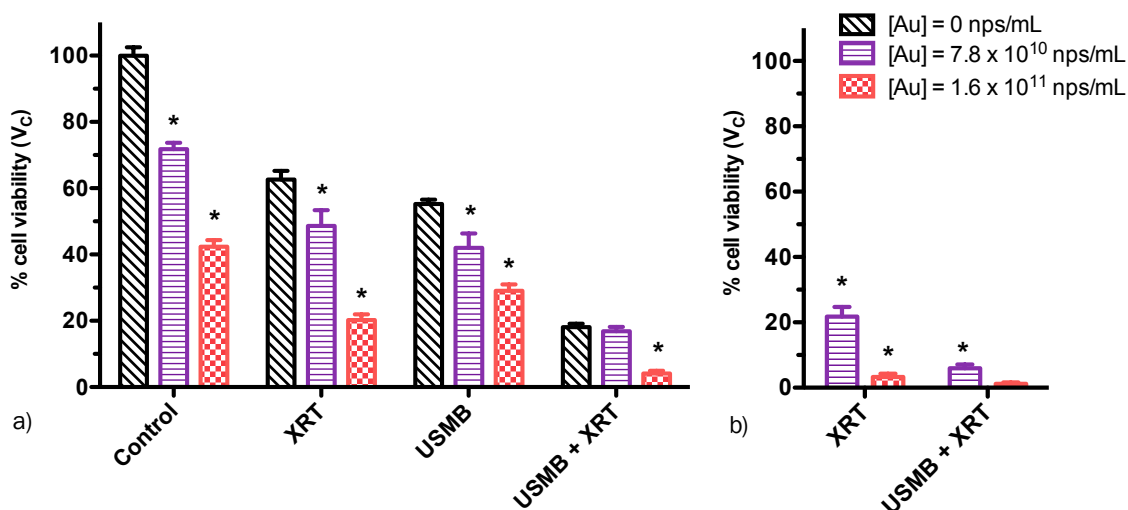


Figure 2.3: Clonogenic viability of MDA-MB231 cells exposed to 12 by 44nm rods shaped AuNPs normalized with control. Two different concentrations of AuNP, USMB fixed at 0.5MHz frequency pulses with 570kPa negative peak pressure and 3.3% (v/v) microbubbles, and a 160kVp 2Gy single radiation dose and their combinations are shown. The asterisks signify its statistical significance in comparison to samples without AuNPs, 0 nps/mL concentration. These samples were centrifuged, removing gold in the solution before irradiation. b) Represents the cell viability of rod shaped AuNPs, USMB, and XRT with gold in solution. The asterisks signify the statistically significant ($P < 0.05$) different to its corresponding treatment without gold in solution in Figure 2.3a).

2.3.3 – Synergism of combined treatments

The calculated additive effect of the combined treatments on cell viability (V_A) with different permutations of AuNP, USMB and XRT using the Bliss independence criterion for spherical and rod-shaped AuNP are shown in Figures 2.4 and 2.5, respectively.

The combined USMB+XRT treatment induced a synergistic effect, as expected, whereas the effect on cell viability was additive with AuNP+USMB as shown in Figures 2.4a) and 2.4b). The effect of AuNP+XRT was synergistic for AuNP spheres and additive at the lower AuNP concentration for rod shaped AuNPs. At the higher concentration of spherical AuNPs, the calculated cell viability ($V_A = 56\%$) was statistically lower compared to experimentally measured cell viability ($V_C = 34\%$) (Figures 2.2a and 2.4a).

The combined treatment of AuNP+USMB+XRT induced a synergistic effect ($V_C=3\%$ at AuNP sphere concentration of 1.6×10^{11} nps/mL) compared with the calculated cell viability ($V_A = 33\%$) based on the experimental cell viability observed with a single treatment (V_C of 87%, 65%, and 58% with AuNP, USMB and XRT, respectively). Both AuNP concentrations with the calculated values from AuNP+USMB+XRT in spherical and rod shaped AuNPs displayed statistical significant differences between the experimental and calculated additive viability, $V_C > V_A$.

The different permutations of the combined treatment of AuNP+USMB+XRT were investigated (Figure 4) to determine the possible synergistic mechanism of a) spherical and b) rod shaped AuNPs by comparing V_C and V_A . Spherical AuNPs in all permutations achieved a synergistic effect at AuNP concentrations of 1.6×10^{11} nps/mL (116nM), however showed no synergistic effect with AuNP concentrations of 7.8×10^{10} nps/mL (60nM) with a V_C of 13% and V_A of 34%. Synergism was only achieved at AuNP concentration of 116nM with the permutation of AuNP+(USMB+XRT) with $V_C= 3\%$ and $V_A= 32\%$. In Figure 4b) rod shaped AuNPs, the combination of (AuNP+XRT)+USMB and (AuNP+USMB)+XRT had $V_C>V_A$ suggesting synergism. However, AuNP+(USMB+XRT) was not

significant in either 7.8×10^{10} nps/mL (152nM) ($V_C = 14\%$, $V_A = 25\%$) and 1.6×10^{11} nps/mL (320nM) ($V_C = 9\%$, $V_A = 15\%$).

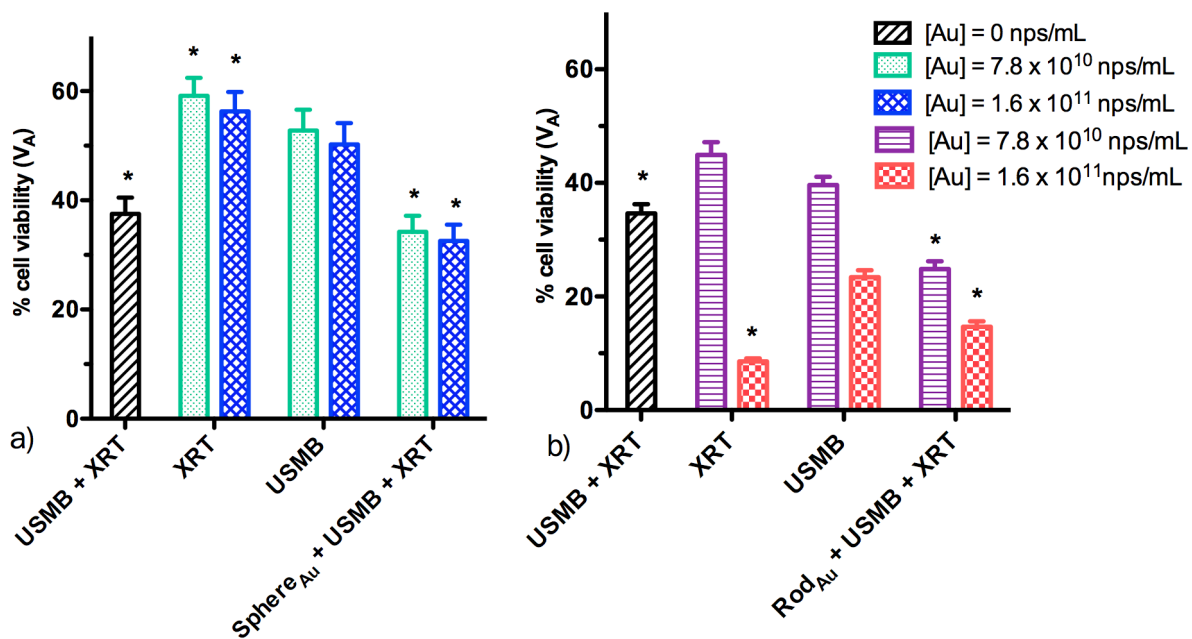


Figure 2.4: The calculated additive effect (V_A) of AuNP, USMB, and XRT on a) spherical AuNPs and b) rod shaped AuNPs. The asterisks identify the treatments that have a statistically significant $V_C > V_A$ with $P < 0.05$.

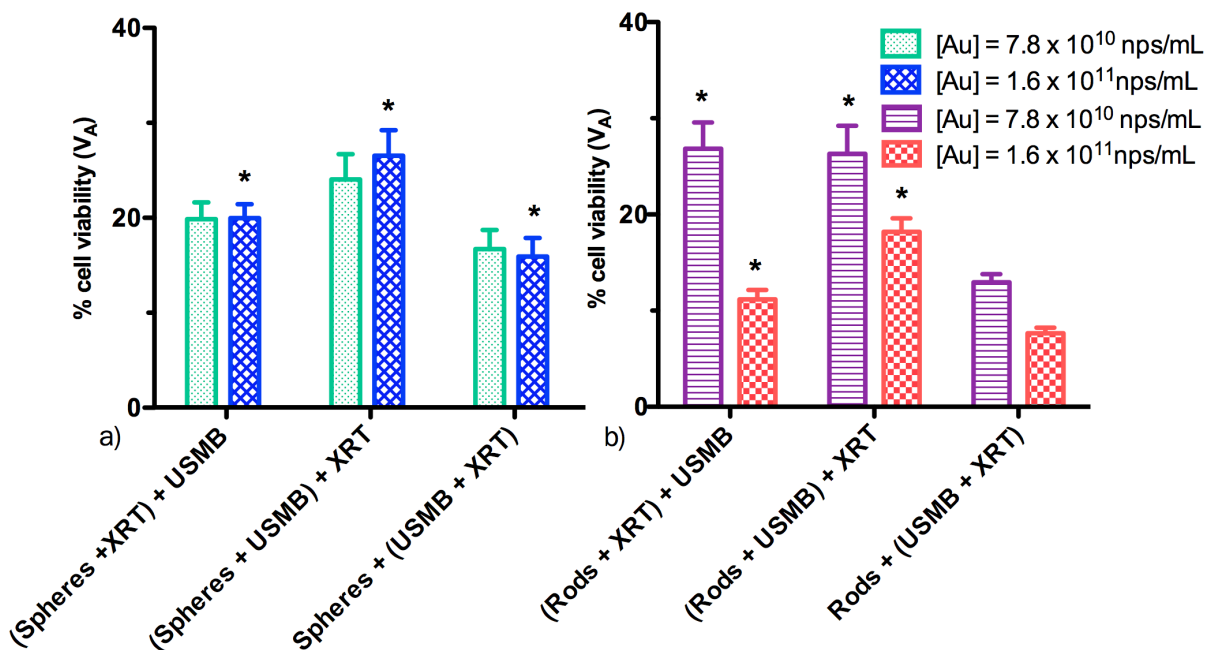


Figure 2.5: The calculated additive effect (V_A) of different permutations of AuNP+USMB+XRT for a) spherical AuNPs and b) rod shaped AuNPs. The asterisks identify the treatments that have a statistically significant $V_C > V_A$ with $P < 0.05$.

2.4 – Discussion

The combined treatment of gold nanoparticles, ultrasound-and-microbubbles, and ionizing radiation improved the therapeutic outcome of radiotherapy by ~22 fold using spherically shaped AuNP of 12nm diameter at a concentration of 116 nM (which corresponds to 1.6×10^{11} nps/mL). It is thought that AuNPs can localize radiation delivery applied in a biological setting or human exposure is possible because of the localized energy deposition. However, clinical applications are mainly limited by the amount of AuNPs that can be administered to the patient and the method of preferentially retaining the AuNPs in cancer cells. Through using ultrasound and microbubbles to deliver AuNPs more efficiently with concentrations of ~ 0.3 – 18,000 fold less compared to other studies, this strategy

has the potential to enter into clinic. In addition, the combination of ultrasound and microbubbles with radiation has been shown to exhibit radiosensitizing properties, further enhancing radiotherapy.

2.4.1 – Gold nanoparticle concentration and location significance

Cell viability with the combined treatment (AuNP+USMB+XRT) depends on gold nanoparticle concentration, size and location. Cell viability of ~3-4% was achieved at concentrations of 1.6×10^{11} nps/mL. Through incubation, more gold nanoparticles can be delivered to cells at higher concentration in the solution (extracellular). However, other studies have shown that AuNPs must be internalized into the tumour cells nucleus in order for Auger electrons to be effective (Cho, 2005; Lechtman et al., 2011). The concentrations used in this study were chosen in a range at the lower range of AuNP concentration (60 – 320 nM) used in other studies to view the potential cell death USMB can provide by increasing uptake. Other concentration dependency studies use concentrations of ~ 0.3 – 18,000 fold more to exhibit an effect (Liu et al., 2010; Trono et al., 2011; Wang et al., 2011; Zhang et al., 2009). In Trono *et al.*, increasing the PEGylated AuNP concentration was able to deliver more AuNP into tumour cells. In solutions with fewer AuNPs, cell receptors are less likely to receive AuNPs, increasing cell membrane wrapping time, which is the time duration for cells to internalize a particle through endocytosis. In addition, low concentrations of AuNPs uptake will not increase with incubation time (Trono *et al.*, 2011). This suggests that low concentration of AuNPs uptake through endocytosis without a method in delivery is improbable. Spherical AuNP+XRT viability did not differ between concentrations with little to no incubation time suggesting uptake through endocytosis. Compared to spheres, rod-shaped AuNP+XRT viability was decreased in with an increase of concentration with no incubation time. However, rod-shaped AuNPs with an aspect ratio of 1:5 was found to have less cellular uptake of rod-shaped AuNPs with lower aspect ratios such as 1:3 (Chithrani *et al.*, 2006), contradicting to the results associate with viability. Although uptake of 1:5 rod-shaped gold may be less, irradiation of nanoparticles that consist of more gold would induce a greater synergistic effect.

AuNPs in the extracellular space significantly enhance radiotherapy at 2Gy with 7.8×10^{10} nps/mL and 1.6×10^{11} nps/mL for AuNP+XRT and AuNP+USMB+XRT allowing <5% cell viability. Gold that remained within the cell suspension post USMB and prior to irradiation decrease in cell viability. The results imply the location of AuNPs does not necessarily need to be within the nucleus for the photoelectric effect and Auger electrons to have an effect. This also suggests a possible trigger for cell death that may be occurring within the cell membrane associated with USMB and radiation, such as up-regulation of ceramide (Al-Mahrouki *et al.*, 2012).

2.4.2 – Mechanism(s) associated with radioenhancement

The synergistic enhancement of cell death with AuNP+USMB+XRT is associated with ultrasound-and-microbubble induced permeabilization of cell membranes (Feril & Kondo, 2004; Schlicher *et al.*, 2006; Stieger *et al.*, 2007) and cause in increase in ceramide production, inducing apoptosis (Al-Mahrouki *et al.*, 2012). Ultrasonically-stimulated microbubbles can generate transient pores within the cell membrane and allow AuNP to enter the cell, which otherwise would be excluded, and results in lower cell viability after radiation. These pores are generally from 30-100nm in size depending on the ultrasound parameters and would be able to accommodate larger AuNPs sizes (Karshafian *et al.*, 2010; Alkilany *et al.*, 2009; Zhou *et al.*, 2008)

In multiple previous *in vitro* and *in vivo* studies, the combination of USMB + XRT mode of cell death was determined to be predominantly apoptosis (Karshafian *et al.*, 2010; Lee *et al.*, 2012). Through gene expression analyses, the treatment revealed an up-regulation of genes known to be involved in apoptosis through ceramide-induced apoptotic pathways (Al-Mahrouki *et al.*, 2012)., Furthermore, genes such as caspase9-alpha and caspase9-beta has been shown to be activated with the combined treatment of USMB+XRT where each treatment alone activated other genes, suggesting a synergism which may attribute to enhanced cell death (Al-Mahrouki *et al.*, 2012). Our results showed ~3 fold decrease in cell viability with USMB+XRT, which agrees with previous studies (Tarapacki *et al.*, 2012; Al-Mahrouki *et al.*, 2012; Czarnota *et al.*, 2012)

Current *in vitro* studies of gold nanoparticles and radiotherapy using surface modified and liposome loaded small AuNPs have demonstrated an enhancement in cell death by ~3 fold (or less) (Kong *et al.*, 2008; Zhang *et al.*, 2008), compared to 22 fold in this study, and enhancement in delivery by ~1000 times (Chithrani *et al.*, 2010; Kong *et al.*, 2008; Zhang *et al.*, 2008). Targeted AuNPs coated with cysteamine and thioglucose delivered through incubation at concentrations of 15nM, have been shown to have a cell viability that was decreased by ~3 folds compared to radiation alone of 10Gy at 200kVp in MCF-7 cells (breast) (Kong *et al.*, 2008). At a more comparable radiation dose, 2Gy at 200kVp, thioglucose and sodium citrate coated 10nm AuNPs were both able to increase cell death by ~ 1.5 folds when incubated for 24 hours at 15nM in DU-145 cells (prostate) (Zhang *et al.*, 2008).

Delivery of AuNPs through liposomes has been shown to increase delivery by 1,000 fold of 1.4 nm spheres (Chithrani *et al.*, 2010). However, liposomes surface properties and stability limits the size of AuNPs that can be used and release time frame. A treatment proficient in delivering larger AuNPs may be preferred to achieve a higher localized radiation dose with an increase in AuNPs delivery. This was observed in the viability of cells exposed AuNPs where rod-shaped gold nanoparticles had more cell death than its spherical counterpart, after radiation. A study that was done without USMB and radiation illustrated and confirmed that rods had a slower uptake in HeLa cells (Chithrani *et al.*, 2006). Viability appears to not be dependent on shape when comparing the combined treatment (AuNP+USMB+XRT) between spherical AuNPs and rod-shaped AuNRs suggesting the aforementioned accommodation to shape with ultrasound and microbubbles. However upon further investigation, with the increased sensitivity caused by USMB+XRT taken into account, no effect was achieved with rod shaped AuNPs at both AuNP concentrations. Spherical AuNP concentration of only 116nM was able to produce a synergistic effect. This suggests that 60nM spherical AuNP concentration was not delivered effectively to produce both radiosensitization and increase in uptake. With respects to rod shaped AuNPs, rods were not able to deliver a statistically significant radioenhancement, making spheres, in comparison, more effective. Uptake of rod shaped nanoparticles of same diameter but different length

may hinder the ability to be taken up by the cell when compared to spherical AuNPs. USMB induced pores are 30-100nm in size, but the distribution of pore size varies with ultrasound parameters and cell type (Czarnota *et al.*, 2012; Karshafian *et al.*, 2010). Since 12nm spherical AuNPs are below the range of pore size, the probability of AuNPs entering the intracellular space of a cell is greater. Together, with the increase of AuNP delivery, and increase radiosensitivity, the results provide an insight on the possible synergistic effects of AuNP, USMB and irradiation and its dependence on size and concentration in an *in vitro* setting.

2.4.3 – AuNP toxicity

The increase of the amount of gold within the cells is correlated with the effectiveness of radiotherapy therefore the use of rod-shaped AuNPs with 12nm width (12x44nm) is preferential (and 3 times greater in volume) to 12nm spheres. However, the byproducts associated with their synthesis may result in unintended consequences. Rod shaped AuNP production requires the use of a structure-directing surfactant known as cetyltrimethylammonium bromide (CTAB) that controls the shape of rod shaped AuNPs. CTAB effects were not present among spherical AuNPs with human breast cancer cells due to its production in citric acid. However, the rod shaped AuNPs precursor CTAB, was toxic to cells at concentrations of ~100 nM. Similar viability studies have been done with Human K562 cells where CTAB was toxic to cells at ~10 nM concentrations (Murphy *et al.*, 2008). The cytotoxicity of rod shaped AuNPs was found to be due to free CTAB and not the rods themselves, or residual metal ions (Alkilany *et al.*, 2009).

2.4.4 – Limitations

In this study, a cell suspension model was used to expose cells to its respective treatments. MDA-MD231 cells are an adherent cell line, which may affect its response if suspended. However, the model used allowed flexible condition manipulation in ultrasound, microbubble concentration, AuNP concentration, and radiation dose. Previous studies have also used similar experimental design (Karshafian *et al.*, 2010; Karshafian & Tchouala, 2010; Ward *et al.*, 2000). Although gold uptake measurements were

not obtained, viability was measured to confirm effectiveness of the combined treatment of AuNP+USMB+XRT. Future work will measure the concentration of the gold inside cells using inductively coupled-plasma mass spectroscopy (ICP-MS) or atomic absorption spectroscopy (AAS) with ~10 ppb and correlate it to the clonogenic data obtained.

2.5 – Conclusions

The combined treatment of gold nanoparticles, ultrasound and microbubbles, and radiation is synergistic in MDA MB231 cells *in vitro*. Cell viability decreased by ~22 fold with the combined treatment compared to XRT alone. The synergistic effects depended on size, concentration, and the location of AuNPs. AuNP concentrations of 116nM spherical were able to decrease cell viability more significantly and rod shaped nanoparticles at 152nM – 320nM AuNP concentrations. Location of AuNPs appeared to play a significant role in decreasing cell viability suggesting additional mechanism causing cell death. Ultrasound and microbubbles also induced a synergistic enhancement with radiation. AuNP and radiation treatments were as expected and also decreased cell viability greater than radiation alone. This study indicates that AuNP+USMB+XRT may significantly enhance the desired effect of radiotherapy and decrease the amount of AuNPs used by increasing delivery resulting in increased radiosensitivity and ultrasound-microbubble induced radiosensitivity.

2.6 – References

- Abuchowski, A., McCoy, J. R., Palczuk, N. C., van Es, T., & Davis, F. F. (1977). Effect of covalent attachment of polyethylene glycol on immunogenicity and circulating life of bovine liver catalase. *The Journal of Biological Chemistry*, 252(11), 3582–3586.
- Al-Mahrouki, A. A., Karshafian, R., Giles, A., & Czarnota, G. J. (2012). Bioeffects of Ultrasound-Stimulated Microbubbles on Endothelial Cells: Gene Expression Changes Associated with Radiation Enhancement in vitro. *Ultrasound in Medicine & Biology*. doi:10.1016/j.ultrasmedbio.2012.07.009
- Alkilany, A. M., Nagaria, P. K., Hexel, C. R., Shaw, T. J., Murphy, C. J., & Wyatt, M. D. (2009). Cellular Uptake and Cytotoxicity of Gold Nanorods: Molecular Origin of Cytotoxicity and Surface Effects. *Small*, 5(6), 701–708. doi:10.1002/smll.200801546
- Bliss, C. I. (2008). The Toxicity of Poisons Applied Jointly. *Annals of Applied Biology*, 26(3), 585–615. doi:10.1111/j.1744-7348.1939.tb06990.x
- Blomley, M. J., Cooke, J. C., Unger, E. C., Monaghan, M. J., & Cosgrove, D. O. (2001). Microbubble contrast agents: a new era in ultrasound. *BMJ (Clinical Research Ed.)*, 322(7296), 1222–1225.
- Bull, J. L. (2007). The application of microbubbles for targeted drug delivery. *Expert Opinion on Drug Delivery*, 4(5), 475–493. doi:10.1517/17425247.4.5.475
- Carter, J. D., Cheng, N. N., Qu, Y., Suarez, G. D., & Guo, T. (2007). Nanoscale energy deposition by X-ray absorbing nanostructures. *The Journal of Physical Chemistry B*, 111(40), 11622–11625. doi:10.1021/jp075253u
- Chattopadhyay, N., Cai, Z., Pignol, J.-P., Keller, B., Lechtman, E., Bendayan, R., & Reilly, R. M. (2010). Design and Characterization of HER-2-Targeted Gold Nanoparticles for Enhanced X-radiation Treatment of Locally Advanced Breast Cancer. *Molecular Pharmaceutics*, 7(6), 2194–2206. doi:10.1021/mp100207t
- Chen, W.-S., Brayman, A. A., Matula, T. J., & Crum, L. A. (2003). Inertial cavitation dose and hemolysis produced in vitro with or without Optison®. *Ultrasound in Medicine & Biology*, 29(5), 725–737. doi:10.1016/S0301-5629(03)00013-9
- Chithrani, B. D., Dunne, M., Stewart, J., Allen, C., & Jaffray, D. J. (2010). Cellular uptake and transport of gold nanoparticles incorporated in a liposomal carrier. *Nanomedicine: Nanotechnology, Biology, and Medicine*, 6(1), 161–169. doi:10.1016/j.nano.2009.04.009
- Chithrani, B. D., Ghazani, A. A., & Chan, W. C. W. (2006). Determining the Size and Shape Dependence of Gold Nanoparticle Uptake into Mammalian Cells. *Nano Letters*, 6(4), 662–668. doi:10.1021/nl052396o

- Cho, S. H. (2005). Estimation of tumour dose enhancement due to gold nanoparticles during typical radiation treatments: a preliminary Monte Carlo study. *Physics in Medicine and Biology*, *50*(15), N163–N173. doi:10.1088/0031-9155/50/15/N01
- Chomas, J. E., Dayton, P., Allen, J., Morgan, K., & Ferrara, K. W. (2001). Mechanisms of contrast agent destruction. *IEEE Transactions on Ultrasonics, Ferroelectrics, and Frequency Control*, *48*(1), 232–248.
- Czarnota, G. J. G., Karshafian, R. R., Burns, P. N. P., Wong, S. S., Al-Mahrouki, A. A., Lee, J. W. J., et al. (2012). Tumor radiation response enhancement by acoustical stimulation of the vasculature. *PNAS*, *109*(30), E2033–E2041. doi:10.1073/pnas.1200053109
- Dreaden, E. C., Mackey, M. A., Huang, X., Kang, B., & El-Sayed, M. A. (2011). Beating cancer in multiple ways using nanogold. *Chemical Society Reviews*, *40*(7), 3391. doi:10.1039/c0cs00180e
- Feril, L. B., Jr, & Kondo, T. (2004). Biological Effects of Low Intensity Ultrasound: The Mechanism Involved, and its Implications on Therapy and on Biosafety of Ultrasound. *Journal of Radiation Research*, *45*(4), 479–489. doi:10.1269/jrr.45.479
- Garcia-Barros, M., Paris, F., Cordon-Cardo, C., Lyden, D., Rafii, S., Haimovitz-Friedman, A., et al. (2003). Tumor response to radiotherapy regulated by endothelial cell apoptosis. *Science*, *300*(5622), 1155–1159. doi:10.1126/science.1082504
- Goorley, T., & Nikjoo, H. (2000). Electron and photon spectra for three gadolinium-based cancer therapy approaches. *Radiation Research*, *154*(5), 556–563. doi:10.1667/0033-7587(2000)154[0556:EAPSFT]2.0.CO;2
- Hainfeld, J. F., Dilmanian, F. A., Slatkin, D. N., & Smilowitz, H. M. (2008). Radiotherapy enhancement with gold nanoparticles. *Journal of Pharmacy and Pharmacology*, *60*(8), 977–985. doi:10.1211/jpp.60.8.0005
- Hainfeld, J. F., Dilmanian, F. A., Zhong, Z., Slatkin, D. N., Kalef-Ezra, J. A., & Smilowitz, H. M. (2010). Gold nanoparticles enhance the radiation therapy of a murine squamous cell carcinoma. *Physics in Medicine and Biology*, *55*(11), 3045–3059. doi:10.1088/0031-9155/55/11/004
- Hainfeld, J. F., Slatkin, D. N., & Smilowitz, H. M. (2004). The use of gold nanoparticles to enhance radiotherapy in mice. *Physics in Medicine and Biology*, *49*(18), N309–N315. doi:10.1088/0031-9155/49/18/N03
- Hainfeld, J. F., Slatkin, D. N., Focella, T. M., & Smilowitz, H. M. (2006). Gold nanoparticles: a new X-ray contrast agent. *British Journal of Radiology*, *79*(939), 248–253. doi:10.1259/bjr/13169882
- Hauck, T. S., Ghazani, A. A., & Chan, W. C. W. (2008). Assessing the Effect of Surface Chemistry on Gold Nanorod Uptake, Toxicity, and Gene Expression in Mammalian Cells. *Small*, *4*(1), 153–159.

doi:10.1002/sml.200700217

- Hernot, S., & Klibanov, A. L. (2008). Microbubbles in ultrasound-triggered drug and gene delivery. *Advanced Drug Delivery Reviews*, 60(10), 1153–1166. doi:10.1016/j.addr.2008.03.005
- Huang, X., & El-Sayed, M. A. (2010). Gold nanoparticles: Optical properties and implementations in cancer diagnosis and photothermal therapy. *Journal of Advanced Research*, 1(1), 13–28. doi:10.1016/j.jare.2010.02.002
- Jain, S., Coulter, J. A., Hounsell, A. R., Butterworth, K. T., McMahon, S. J., Hyland, W. B., et al. (2011). Cell-specific radiosensitization by gold nanoparticles at megavoltage radiation energies. *International Journal of Radiation Oncology, Biology, Physics*, 79(2), 531–539. doi:10.1016/j.ijrobp.2010.08.044
- Jokerst, J. V., Lobovkina, T., Zare, R. N., & Gambhir, S. S. (2011). Nanoparticle PEGylation for imaging and therapy. *Nanomedicine*, 6(4), 715–728. doi:10.2217/nnm.11.19
- Karshafian, R. (2009). On the Permeabilisation and Disruption of Cell Membranes by Ultrasound and Microbubbles, 1–123.
- Karshafian, R., & Tchouala, J. I. N. (2010). Enhancement of Radiation Therapy by Ultrasonically-stimulated Microbubbles In Vitro: Effects of Treatment Scheduling on Cell Viability and Production of Ceramide. *Ultrasonics Symposium (IUS), 2010*, 2115–2118. doi:10.1109/ULTSYM.2010.0534
- Karshafian, R., Bevan, P. D., Williams, R., Samac, S., & Burns, P. N. (2009). Sonoporation by Ultrasound-Activated Microbubble Contrast Agents: Effect of Acoustic Exposure Parameters on Cell Membrane Permeability and Cell Viability. *UMB*, 35(5), 847–860. doi:10.1016/j.ultrasmedbio.2008.10.013
- Karshafian, R., Samac, S., Bevan, P. D., & Burns, P. N. (2010). Microbubble mediated sonoporation of cells in suspension: Clonogenic viability and influence of molecular size on uptake. *Ultrasonics*, 50(7), 691–697. doi:10.1016/j.ultras.2010.01.009
- Keller, M. W., Segal, S. S., Kaul, S., & Duling, B. (1989). The behavior of sonicated albumin microbubbles within the microcirculation: a basis for their use during myocardial contrast echocardiography. *Circulation Research*, 65(2), 458–467.
- Kennedy, J. E. (2003). High intensity focused ultrasound: surgery of the future? *British Journal of Radiology*, 76(909), 590–599. doi:10.1259/bjr/17150274
- Kennedy, L. C., Bear, A. S., Young, J. K., Lewinski, N. A., Kim, J., Foster, A. E., & Drezek, R. A. (2011). T cells enhance gold nanoparticle delivery to tumors in vivo. *Nanoscale Research Letters*, 6(1), 283. doi:10.1186/1556-276X-6-283
- Kinsella, T. J., Schupp, J. E., Davis, T. W., Berry, S. E., Hwang, H. S., Warren, K., et al. (2000).

- Preclinical study of the systemic toxicity and pharmacokinetics of 5-iodo-2-deoxypyrimidinone-2'-deoxyribose as a radiosensitizing prodrug in two, non-rodent animal species: implications for phase I study design. *Clinical Cancer Research*, 6(9), 3670–3679.
- Kolios, M. C., Czarnota, G. J., Lee, M., Hunt, J. W., & Sherar, M. D. (2002). Ultrasonic spectral parameter characterization of apoptosis. *Umb*, 28(5), 589–597.
- Kong, T., Zeng, J., Wang, X., Yang, X., Yang, J., McQuarrie, S., et al. (2008). Enhancement of Radiation Cytotoxicity in Breast-Cancer Cells by Localized Attachment of Gold Nanoparticles. *Small*, 4(9), 1537–1543. doi:10.1002/smll.200700794
- Lechtman, E., Chattopadhyay, N., Cai, Z., Mashouf, S., Reilly, R., & Pignol, J. P. (2011). Implications on clinical scenario of gold nanoparticle radiosensitization in regards to photon energy, nanoparticle size, concentration and location. *Physics in Medicine and Biology*, 56(15), 4631–4647. doi:10.1088/0031-9155/56/15/001
- Lee, J., Karshafian, R., Papanicolau, N., Giles, A., Kolios, M. C., & Czarnota, G. J. (2012). Quantitative Ultrasound for the Monitoring of Novel Microbubble and Ultrasound Radiosensitization. *Umb*, 38(7), 1212–1221. doi:10.1016/j.ultrasmedbio.2012.01.028
- Lentacker, I., De Smedt, S. C., & Sanders, N. N. (2009). Drug loaded microbubble design for ultrasound triggered delivery. *Soft Matter*, 5(11), 2161. doi:10.1039/b823051j
- Liang, H.-D., Tang, J., Halliwell, M., & Wells, P. N. T. (2009). Sonoporation, drug delivery, and gene therapy. *Proceedings of the Institution of Mechanical Engineers, Part H: Journal of Engineering in Medicine*, 224(2), 343–361. doi:10.1243/09544119JEIM565
- Liu, C.-J., Wang, C.-H., Chen, S.-T., Chen, H.-H., Leng, W.-H., Chien, C.-C., et al. (2010). Enhancement of cell radiation sensitivity by pegylated gold nanoparticles. *Physics in Medicine and Biology*, 55(4), 931–945. doi:10.1088/0031-9155/55/4/002
- Matsudaira, H., Ueno, A. M., & Furuno, I. (1980). Iodine contrast medium sensitizes cultured mammalian cells to X rays but not to gamma rays. *Radiation Research*, 84(1), 144–148.
- McDonald, D. M., & Baluk, P. (2002). Significance of blood vessel leakiness in cancer. (Vol. 62, pp. 5381–5385). Presented at the Cancer research.
- McMahon, S. J., Mendenhall, M. H., Jain, S., & Currell, F. (2008). Radiotherapy in the presence of contrast agents: a general figure of merit and its application to gold nanoparticles. *Physics in Medicine and Biology*, 53(20), 5635–5651. doi:10.1088/0031-9155/53/20/005
- Mears, S., & Alonso, A. (2007). Ultrasound, microbubbles and the blood-brain barrier. *Progress in Biophysics and Molecular Biology*, 93(1-3), 354–362. doi:10.1016/j.pbiomolbio.2006.07.019
- Mello, R. R. S., Callisen, H. H., Winter, J. J., Kagan, A. R. A., & Norman, A. A. (1983). Radiation dose

- enhancement in tumors with iodine. *Medical Physics*, 10(1), 75–78.
- Mesbahi, A. (2010). A review on gold nanoparticles radiosensitization effect in radiation therapy of cancer. *Reports of Practical Oncology & Radiotherapy*, 15(6), 176–180.
doi:10.1016/j.rpor.2010.09.001
- Murphy, C. J., Gole, A. M., Stone, J. W., Sisco, P. N., Alkilany, A. M., Goldsmith, E. C., & Baxter, S. C. (2008). Gold Nanoparticles in Biology: Beyond Toxicity to Cellular Imaging. *Accounts of Chemical Research*, 41(12), 1721–1730. doi:10.1021/ar800035u
- Pan, Y., Neuss, S., Leifert, A., Fischler, M., Wen, F., Simon, U., et al. (2007). Size-dependent cytotoxicity of gold nanoparticles. *Small*, 3(11), 1941–1949. doi:10.1002/smll.200700378
- Pignol, J.-P., Rakovitch, E., Beachey, D., & Le Sech, C. (2003). Clinical significance of atomic inner shell ionization (ISI) and Auger cascade for radiosensitization using IUdR, BUdR, platinum salts, or gadolinium porphyrin compounds. *International Journal of Radiation Oncology, Biology, Physics*, 55(4), 1082–1091.
- Polf, J. C., Bronk, L. F., Driessen, W. H. P., Arap, W., Pasqualini, R., & Gillin, M. (2011). Enhanced relative biological effectiveness of proton radiotherapy in tumor cells with internalized gold nanoparticles. *Applied Physics Letters*, 98(19), 193702. doi:10.1063/1.3589914
- Popovtzer, R., Agrawal, A., Kotov, N. A., Popovtzer, A., Balter, J., Carey, T. E., & Kopelman, R. (2008). Targeted Gold Nanoparticles Enable Molecular CT Imaging of Cancer. *Nano Letters*, 8(12), 4593–4596. doi:10.1021/nl8029114
- Rotolo, J. J., Stancevic, B. B., Zhang, J. J., Hua, G. G., Fuller, J. J., Yin, X. X., et al. (2012). Anti-ceramide antibody prevents the radiation gastrointestinal syndrome in mice. *Journal of Clinical Investigation*, 122(5), 1786–1790. doi:10.1172/JCI59920
- Rychak, J. J., Klivanov, A. L., Ley, K. F., & Hossack, J. A. (2007). Enhanced targeting of ultrasound contrast agents using acoustic radiation force. *Ultrasound in Medicine & Biology*, 33(7), 1132–1139. doi:10.1016/j.ultrasmedbio.2007.01.005
- Schlicher, R. K., Radhakrishna, H., Tolentino, T. P., Apkarian, R. P., Zarnitsyn, V., & Prausnitz, M. R. (2006). Mechanism of intracellular delivery by acoustic cavitation. *Ultrasound in Medicine & Biology*, 32(6), 915–924. doi:10.1016/j.ultrasmedbio.2006.02.1416
- Stieger, S. M., Caskey, C. F., Adamson, R. H., Qin, S., Curry, F. R. E., Wisner, E. R., & Ferrara, K. W. (2007). Enhancement of Vascular Permeability with Low-Frequency Contrast-enhanced Ultrasound in the Chorioallantoic Membrane Model. *Radiology*, 243(1), 112–121.
doi:10.1148/radiol.2431060167

- Tarapacki, C., Kumaradas, J. C., & Karshafian, R. (2012). Enhancing laser thermal-therapy using ultrasound-microbubble and gold nanorods of in vitro cells. *Ultrasonics*. doi:10.1016/j.ultras.2012.11.006
- Trono, J. D., Mizuno, K., Yusa, N., Matsukawa, T., Yokoyama, K., & Uesaka, M. (2011). Size, Concentration and Incubation Time Dependence of Gold Nanoparticle Uptake into Pancreas Cancer Cells and its Future Application to X-ray Drug Delivery System. *Journal of Radiation Research*, 52(1), 103–109. doi:10.1269/jrr.10068
- Wang, C.-H., Liu, C.-J., Chien, C.-C., Chen, H.-T., Hua, T.-E., Leng, W.-H., et al. (2011). X-ray synthesized PEGylated (polyethylene glycol coated) gold nanoparticles in mice strongly accumulate in tumors. *Materials Chemistry and Physics*, 126(1-2), 352–356. doi:10.1016/j.matchemphys.2010.11.014
- Ward, M., Wu, J., & Chiu, J. F. (2000). Experimental study of the effects of Optison concentration on sonoporation in vitro. *Umb*, 26(7), 1169–1175.
- Webb, S. (2003). The physical basis of IMRT and inverse planning. *British Journal of Radiology*, 76(910), 678–689. doi:10.1259/bjr/65676879
- Yih, T. C., & Wei, C. (2005). Nanomedicine in cancer treatment. *Nanomedicine: Nanotechnology, Biology, and Medicine*, 1(2), 191–192. doi:10.1016/j.nano.2005.04.001
- Yu, C. X., & Tang, G. (2011). Intensity-modulated arc therapy: principles, technologies and clinical implementation. *Physics in Medicine and Biology*, 56(5), R31–54. doi:10.1088/0031-9155/56/5/R01
- Zhang, X., Xing, J. Z., Chen, J., Ko, L., Amanie, J., Gulavita, S., et al. (2008). Enhanced radiation sensitivity in prostate cancer by gold-nanoparticles (Vol. 31, pp. E160–E167). Presented at the Clinical and Investigative Medicine.
- Zhang, X.D., Guo, M.-L., Wu, H.Y., Sun, Y.M., Ding, Y.Q., Feng, X., & Zhang, L.A. (2009). Irradiation stability and cytotoxicity of gold nanoparticles for radiotherapy. *International Journal of Nanomedicine*, 4, 165–173.
- Zhou, Y., Kumon, R. E., Cui, J., & Deng, C. X. (2009). The Size of Sonoporation Pores on the Cell Membrane. *Umb*, 35(10), 1756–1760. doi:10.1016/j.ultrasmedbio.2009.05.012
- Zhou, Y., Shi, J., Cui, J., & Deng, C. X. (2008). Effects of extracellular calcium on cell membrane resealing in sonoporation. *Journal of Controlled Release*, 126(1), 34–43. doi:10.1016/j.jconrel.2007.11.007

2.7 – Appendix

Table 2.1: A summary of the Bliss independence criterion T-test comparison (shown in Figure 2.4 and Figure 2.5) on spherical AuNPs where ✓ represents synergistic effects, and + represents additive effects.

Conditions	AuNP Concentration [nps/mL]		
	0	7.8×10^{10}	16×10^{10}
USMB + XRT	✓	n/a	n/a
AuNP + XRT	n/a	+	+
AuNP + USMB	n/a	+	+
AuNP + USMB + XRT	n/a	✓	✓
(AuNP + XRT) + USMB	n/a	+	✓
(AuNP + USMB) + XRT	n/a	+	✓
AuNP + (USMB + XRT)	n/a	+	✓

Table 2.2: A summary of the Bliss independence criterion T-test comparison (shown in Figure 2.4 and 2.5) on rod shaped AuNPs where ✓ represents synergistic effects, and + represents additive effects.

Conditions	AuNP Concentration [nps/mL]		
	0	7.8×10^{10}	16×10^{10}
USMB + XRT	✓	n/a	n/a
AuNP + XRT	n/a	+	✓
AuNP + USMB	n/a	+	+
AuNP + USMB + XRT	n/a	✓	✓
(AuNP + XRT) + USMB	n/a	✓	✓
(AuNP + USMB) + XRT	n/a	✓	✓
AuNP + (USMB + XRT)	n/a	+	+

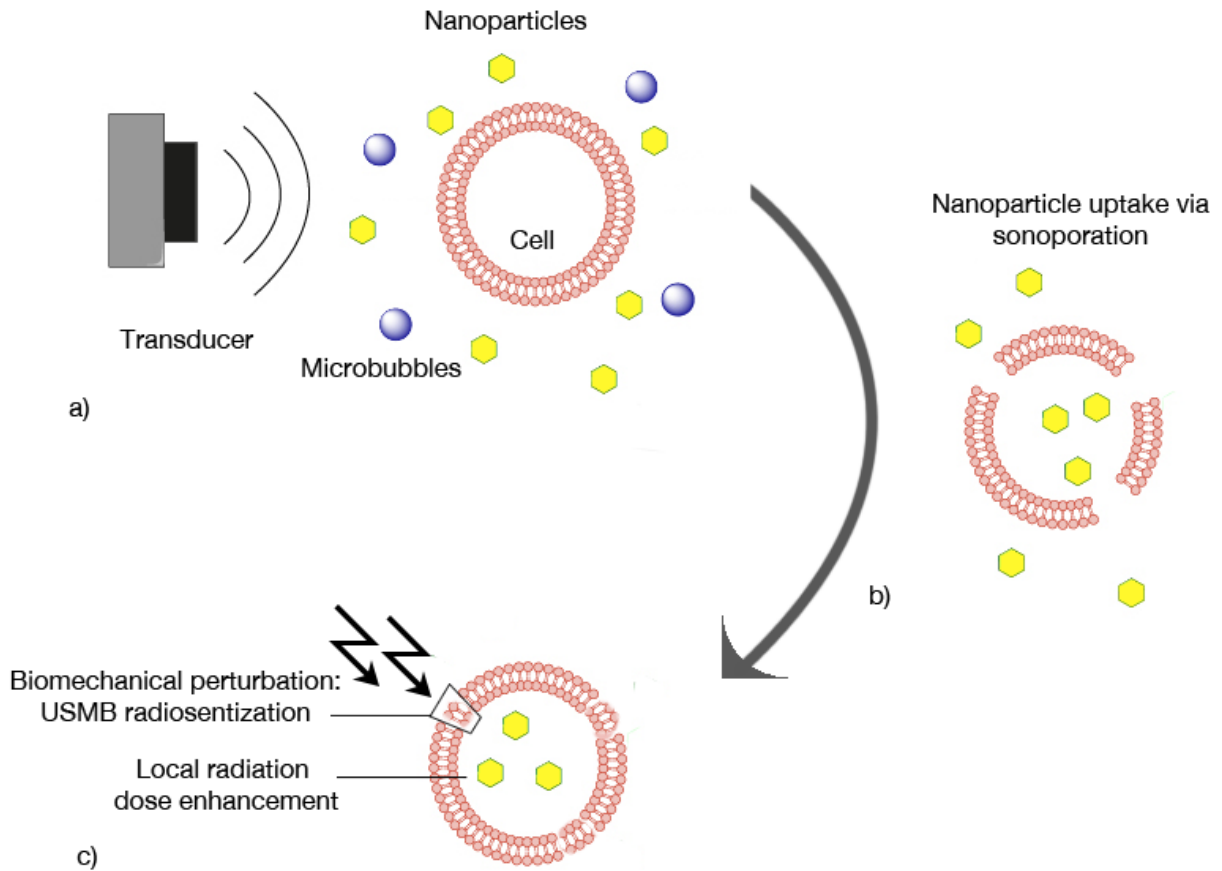


Figure 2.1i – Schematic of possible biomechanisms occurring during the combined treatment of AuNP+USMB+XRT. a) The nanoparticle, microbubble, and cell suspension is exposed to ultrasound, causing b) sonoporation to occur, aiding in uptake. This increase in uptake c) improves local dose delivery and USMB radiosensitization, upon radiation to increase cell death.

Chapter 3

SUMMARY & FUTURE WORK

3.1 – Summary

Gold nanoparticles can increase the local dose of radiation. However, delivery of AuNPs at high concentrations remains a challenge, limiting its application. In our study, ultrasound and microbubbles were used to increase delivery and was combined with AuNP+XRT. In addition, to utilizing the phenomenon of sonoporation caused by the microbubble oscillations, it was demonstrated that ultrasound and microbubbles with radiation causes an increase in cell death suggesting a synergistic effect. A cell suspension model was exposed to combinations of AuNP+USMB+XRT and was accessed with clonogenic assay. The clonogenic viability data suggest that the combined treatment of AuNP+USMB+XRT with spherical 12nm gold nanoparticles at 116nM concentrations produced the greatest cell death.

Many factors were considered. The size, shape, concentration, and location of the gold nanoparticles played a significant role in the treatments effectiveness. Breast cancer cells were able to take up spherical AuNPs more efficiently with the combined treatment compared to rod shaped AuNPs. AuNPs that were within the solution in comparison to without exhibited a statistically significant

decrease in cell viability suggesting a possible mechanism associated with AuNPs and the plasma membrane with the combined treatment. Through the Bliss independence criterion, concentrations of both high and low displayed synergistic properties in both rod shaped and spherical AuNPs, but are more pronounced among spheres. Due to the significantly lower AuNP concentrations used, this strategy has the potential to enter into clinic enhancing both AuNP uptake and increasing radiosensitivity through the Auger cascade and ultrasound microbubble induced sensitivity. This project was among the first to demonstrate the increase in cell death with the combined treatment of AuNP + USMB + XRT.

3.2 – Future work

The purpose of investigating synergism is to evaluate the effectiveness of a treatment and provide a possible insight of the mechanism. This was done *in vitro* to eliminate possible factors that may hinder its achievable radiosensitivity and increase in uptake.

The main practical differences between cell and animal drug combinations studies are (a) animal experiments are more expensive, (b) more time-consuming, (c) more factors that attribute to variability, and (d) smaller population size. For anticancer drug combination studies against xenograft tumours in SCID mice under optimal therapeutic conditions, only 76 mice were used to determine synergy. By contrast, using clonogenic assay, 500 + dishes were used for a statistically significant sample size with more experimental control. Although *in vitro* models provide a solid basis, these models only reveal side effects on a molecular level and cannot reveal side effects like tumour vasculature and possible responses to treatment at a macroscopic scale.

Using similar exposure conditions in an animal model with PEGylated AuNPs can provide understand of the transferability of ultrasound conditions, as well as its proven synergism among spherical AuNPs shown in Chapter 2.

3.1 – Material and Methods: *in vivo* animal model

MDA MB 231 cells were xenografted on the hind leg of severe combined immunodeficient (SCID) mice and treated with combinations of AuNP+USMB+XRT. The mice were euthanized and its tumour was extracted for histology post 24 hours. Low and higher frequency ultrasound images were obtained with RF signal data and power Doppler for the detection of blood within the tumour. Each condition consisted of 4 mice, with a total of 76 mice used for this study.

3.1.1 – In vivo animal model

The Animal Use Protocol for this study, approved by the Sunnybrook Research Institute Animal Care Committee (SRI ACC), and procedures were conducted in accordance with the Canadian Council on Animal Care Guidelines. Female SCID mice (Charles River Laboratory International Inc. Canada) were used. A total volume of 50 microliters of the prepared cell suspension was injected subcutaneously into the right hind leg of each mouse, using a 27 gauge needle. During injections mice were anaesthetized using oxygen ventilated isoflurane. Sizable (8-12mm diameter) tumours formed 4-6 weeks post injections were used for experimentation.

Prior to treatment, mice were anaesthetized using a mixture of Ketamine (100mg/kg), Xylazine (5m/kg) and Acepromazine (1mg/kg), administered intraperitoneally. Anaesthetized mice were visually monitored and placed under heat lamps and/or over warmed pads to maintain regular body temperature during treatment. Mice observed to experience irregular respiratory rates were administered oxygen. Lubrication was also applied to the eyes. Post treatment, mice were given a 0.5mL saline flush injection.

3.1.2 – Gold nanoparticles (AuNP)

Nanocs Inc (New York, USA) PEG coated with molecular weight of 5000Da and a size of 50nm radius spheres were used. The AuNPs were injected through a tail-vein catheter and was administered 1.4 - 3.8mg/kg of gold.

3.1.3 – Ultrasound and microbubble treatment

Mice were immersed in a 37°C water tank with its tumour centered and at the focus of the ultrasound treatment. The ultrasound exposure system consisted of a single element transducer of 500 kHz center-frequency (IL0509HP, Valpey Fisher Inc., Hopkinton, MA) mounted to a micro-positioning system, a waveform generator (AWG520, Tektronix Inc., Beaverton, OR) and a power amplifier (RPR4000, Ritec Inc., Warwick, RI). The mice were exposed to ultrasound pulses at 32µs pulse duration, 1kHz pulse repetition frequency, and a 5 minute treatment (compared to 60s *in vitro*) time at 570kPa negative peak pressure based on previous sonoporation experiments (Czarnota: et al., 2012) Definity® (Lantheus Medical Imaging, Inc., North Billerica, MA, USA) microbubbles at a concentration of 3.3% v/v (volume concentration) was used. The microbubbles were introduced through a tail-vein catheter using 100µL of microbubbles and 50µL saline flush. The agent was allowed to reach room temperature prior to activation.

3.1.4 – Radiotherapy (XRT)

Following ultrasound treatment, the mouse was lead-shielded and its tumour was exposed to an 8Gy single fraction dose at 160kVp and 200cGy/min dose rate (Faxitron Xray Corporation, Lincolnshire, IL, USA).

3.1.5 – Growth Delay

SCID mice were measured 3 times a week post treatment with a calliper until tumour hindered the mice mobility. The mice were then euthanized by means of cervical dislocation. Tumour volume was determined using $(l \times w \times h \times \pi)/6$ to account for its spherical shape.

3.1.6 – Histology

Samples were fixed for 24 hours in 1% paraformaldehyde, and embedded in paraffin blocks. Tumour sections were cut from distal to proximal ends of the tumour. Slices were cytospinned at 2000 x g and fixed for 30 minutes. Standard hematoxylin and eosin staining was done.

3.1.7 – Ultrasound Imaging

A VEVO 770 (Visualsonics, Toronto, Canada) was used to obtain b-mode, power Doppler, and RF signal data pre and post 24 hours of treatment. The mouse was anesthetised and secured onto an acrylic glass stage with its hind leg immersed in degassed water. The scans began from the upper leg and moved towards the foot using a motorized micro-positioning system that provided multiple parallel cross section images of the tumour. The option of a power Doppler mode was used with an RMV707b transducer at 20MHz central frequency. The image was taken using a step size of 0.2mm, a wall filter of 2.0 mm/s, and a scan speed of 2.0 mm/s. RF data was also acquired, collecting 250 RF lines per image. This data is in the process of being analyzed.

3.2 – Results & Discussion

PEG-AuNPs were used for this study to avoid unwanted opsonization by macrophages and allow more AuNPs to be taken up to its targeted region.

3.2.1 – Histology images

The hematoxylin and eosin (H&E) stains indicate sparse, small regions of decreased apparent cell density, suggesting cell death and necrosis within the all conditions, including the control (Figure 3.1). This signifies a necrotic core prior to treatment and will be taken into account when observing other conditions. The size of the necrotic core correlated with the increase in treatments. AuNP, USMB and AuNP+USMB show comparable death cell regions. A significant increase in sparse tissue is observed with AuNP+USMB+XRT compared with AuNP+XRT and USMB+XRT. This promotes and emphasizes the potential of the combined treatment of AuNP+USMB+XRT.

AuNP concentration was varied with the combined treatment (Figure 3.2) and exhibited an increase in sparse apparent cell density as AuNP concentration increased. AuNP concentration of 2.8mg/kg and 3.8mg/kg showed comparable results. This confirms the importance of AuNP concentrations on the combined treatment's effectiveness.

Further analysis will be done on selected conditions via TUNEL, KI67, and CD31 staining to observed DNA fragmentation due to apoptosis and to determine mode of tumour cell death and blood vessel activity.

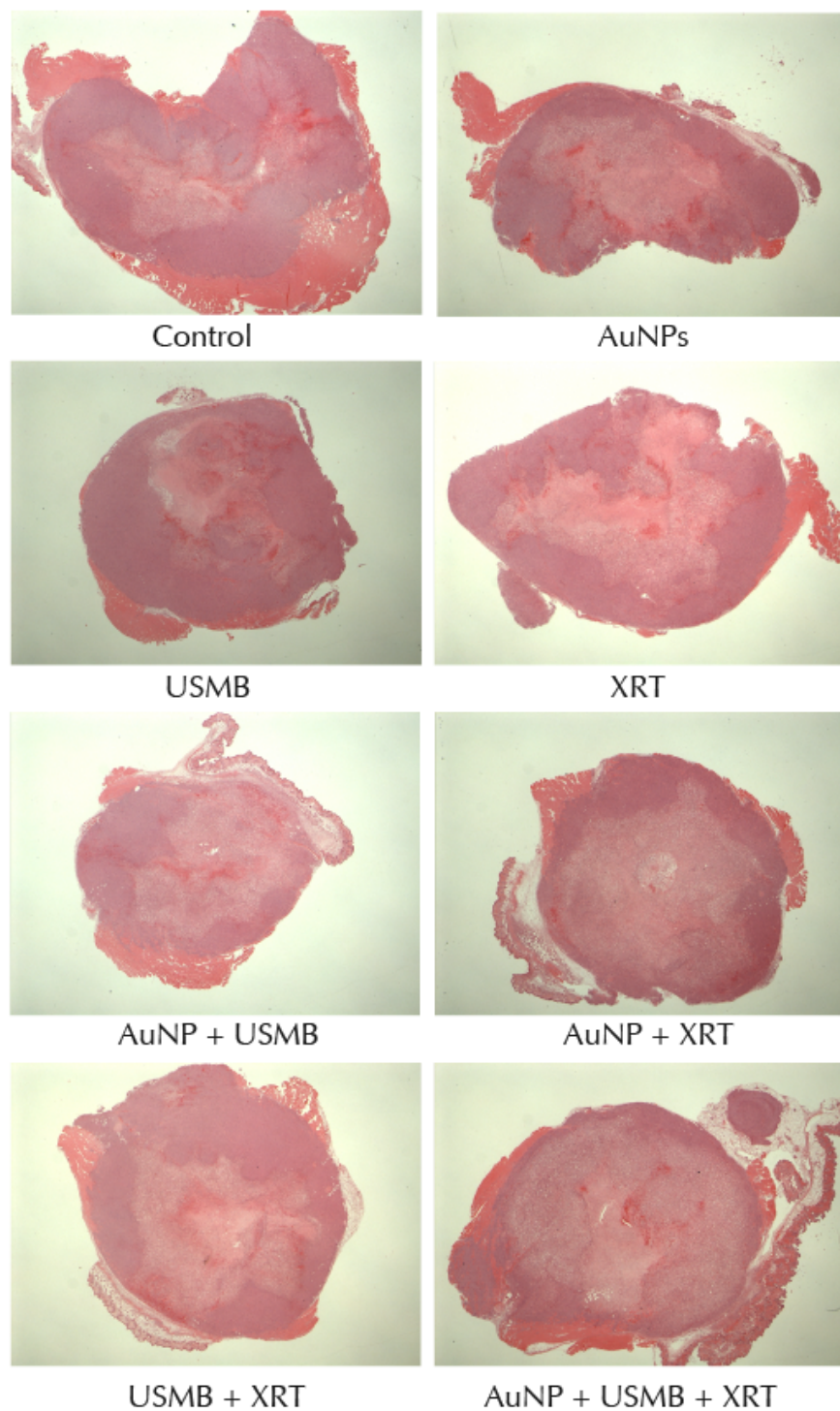
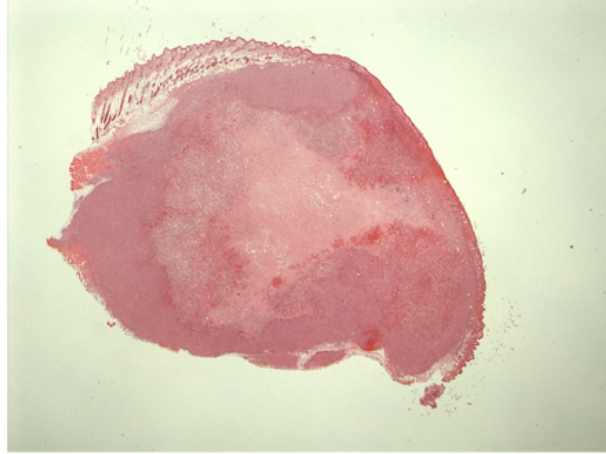
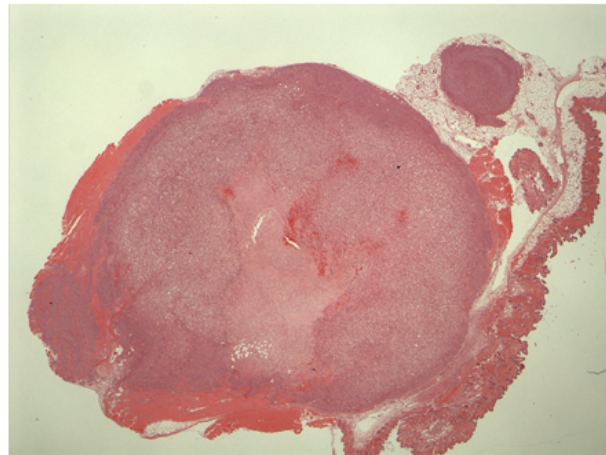


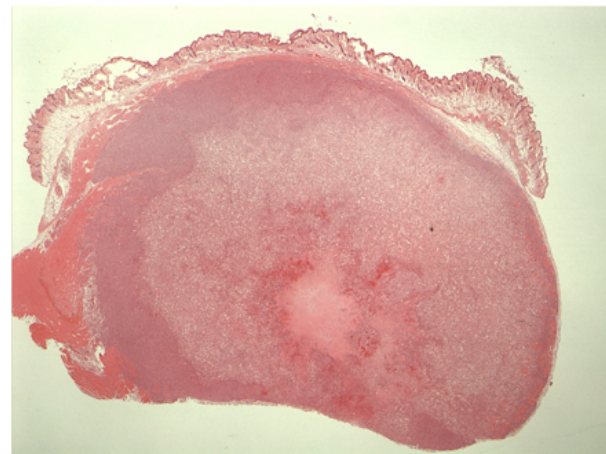
Figure 3.1: Representative hematoxylin and eosin stains for the untreated control, AuNPs, USMB, XRT, AuNP+USMB, AuNP+XRT, USMB+XRT, and AuNP+USMB+XRT. Images were taken at 1x magnification with a light microscope.



1.4 mg/kg of AuNP + USMB + XRT



2.8 mg/kg of AuNP + USMB + XRT



3.8 mg/kg of AuNP + USMB + XRT

Figure 3. 2: H&E stains of MDA-MB 231 mice tumours with different AuNP concentrations used with the combined treatment of AuNP+USMB+XRT. From top to bottom: 1.4mg/kg, 2.8mg/kg, and 3.8mg/kg of 50nm spherical PEG-AuNP used with the combined treatment with ultrasound and microbubbles and radiation (n=4). Images were taken at 1x magnification with a light microscope.

3.2.2 – Growth Delay

A growth delay study was performed with 20 mice in total with 4 mice per condition. The control group of mice increased in tumour size through time significantly in comparison to all other groups as expected (Figure 3.3). Mice exposed to radiation inhibited tumour growth for ~21 days and eventually increased in size. AuNP+XRT reveal a postponed growth in tumour compared to XRT alone. USMB+XRT and AuNP+USMB+XRT demonstrate a similar curve. Both curves suggest a prolonged suppressed tumour growth beyond condition groups of: the untreated control, XRT, AuNP+XRT. At day 28, a mouse was euthanized within the condition group of USMB+XRT, causing a sharp decrease in tumour volume.

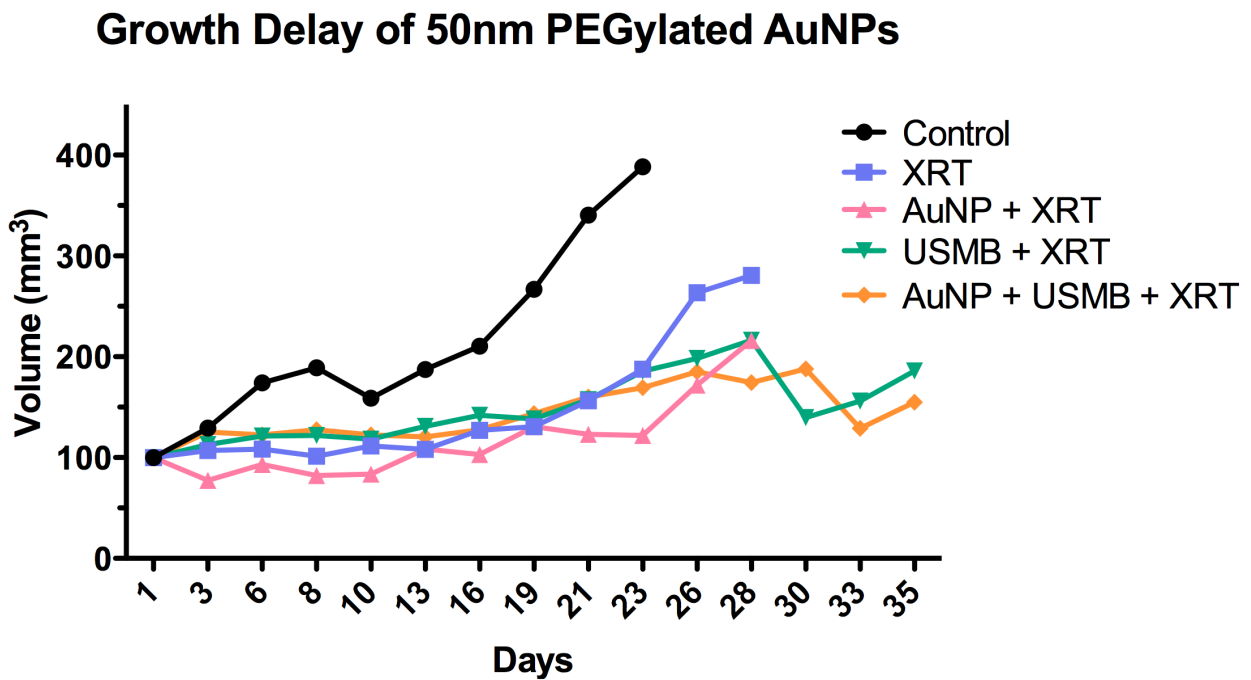


Figure 3.3: Growth delay curve of tumour growth post treatments normalized with untreated control (n=4). All microbubble treatments were done with 3% (v/v), with an AuNP dose of 2.8mg/kg and 2Gy X-ray radiation.

The addition of AuNP demonstrates a postponed growth in tumours in both AuNP+XRT and AuNP+USMB+XRT. USMB+XRT also delayed tumour growth, similar to that of the combined treatment

with similar tumour size implying AuNPs little effect. However, H&E stains indicate that AuNP+USMB+XRT has a larger area of tumour cell death paralleled with USMB+XRT. In addition, increasing AuNP concentration with the combined treatment appeared to increase the amount of sparsely dense tissue.

The combined treatment in this study relies on ultrasound administered in the presence of microbubbles and AuNPs, followed by irradiation to induced cell death. Our recent observations indicate that such treatment enhances the effect of radiation on cells and endothelial cells, inducing possible apoptotic cell death. Further analysis will be done using the high and low frequency b-mode images, as well as power Doppler to detect blood within the tumour before and 24 hours after treatment.

3.2.3 – References

Czarnota, G. J. G., Karshafian, R. R., Burns, P. N. P., Wong, S. S., Al-Mahrouki, A. A., Lee, J. W. J., et al. (2012). Tumor radiation response enhancement by acoustical stimulation of the vasculature. *PNAS*, *109*(30), E2033–E2041. doi:10.1073/pnas.1200053109